Topology, cross-frequency, and same-frequency band interactions shape the generation of phase-amplitude coupling in a neural mass model of a cortical column

Roberto C. Sotero

Hotchkiss Brain Institute, Department of Radiology, University of Calgary, Calgary, AB, Canada

Correspondence: Roberto C. Sotero, Department of Radiology and Hotchkiss Brain Institute, University of Calgary, 3330 Hospital Drive NW, HSC Building, Room 2923. Calgary, Alberta, T2N 4N1. Canada

roberto.soterodiaz@ucalgary.ca

Abstract

Phase-amplitude coupling (PAC), a type of cross-frequency coupling (CFC) where the phase of a low-frequency rhythm modulates the amplitude of a higher frequency, is becoming an important indicator of information transmission in the brain. However, the neurobiological mechanisms underlying its generation remain undetermined. A realistic, yet tractable computational model of the phenomenon is thus needed. Here we propose a neural mass model of a cortical column, comprising fourteen neuronal populations distributed across four layers (L2/3, L4, L5 and L6). The conditional transfer entropies (cTE) from the phases to the amplitudes of the generated oscillations are estimated by means of the conditional mutual information. This approach provides information regarding directionality by distinguishing PAC from APC (amplitude-phase coupling), i.e. the information transfer from amplitudes to phases, and can be used to estimate other types of CFC such as amplitude-amplitude coupling (AAC) and phase-phase coupling (PPC). While experiments often only focus on one or two PAC combinations (e.g., theta-gamma or alpha-gamma), we found that a cortical column can simultaneously generate almost all possible PAC combinations, depending on connectivity parameters, time constants, and external inputs. We found that the strength of PAC between two populations was strongly correlated with the strength of the effective connections between them and, on average, did not depend upon the presence or absence of a direct (anatomical) connection. When considering a cortical column circuit as a complex network, we found that neuronal populations making indirect PAC connections had, on average, higher local clustering coefficient, efficiency, and betweenness centrality than populations making direct connections and populations not involved in PAC connections. This suggests that their interactions were more efficient when transmitting information. Since more than 60% of the obtained interactions represented indirect connections,

our results highlight the importance of the topology of cortical circuits for the generation of the PAC phenomenon. Finally, our results demonstrated that indirect PAC interactions can be explained by a cascade of direct CFC and same-frequency band interactions, suggesting that PAC analysis of experimental data should be accompanied by the estimation of other types of frequency interactions for an integrative understanding of the phenomenon.

Keywords: neural mass models; phase-amplitude coupling; cross-frequency coupling; cortical column; conditional mutual information; conditional transfer entropy; complex networks

1. Introduction

It has been hypothesized that phase-amplitude coupling (PAC) of neurophysiological signals plays a role in the shaping of local neuronal oscillations and in the communication between cortical areas (Canolty and Knight 2010). PAC occurs when the phase of a low frequency oscillation modulates the amplitude of a higher frequency oscillation. A classic example of this phenomenon was demonstrated in the CA1 region of the hippocampus (Bragin, Jando et al. 1995), where the phase of the theta band modulated the power of the gamma-band. Computational models of the theta-gamma PAC generation in the hippocampus have been proposed (Kopell, Boergers et al. 2010) and are based on two main types of models. The first type of models consists of a network of inhibitory neurons (I-I model) (White, Banks et al. 2000), whereas the second model is based on the reciprocal connections between networks of excitatory pyramidal cells and inhibitory neurons (E-I model) (Tort, Rotstein et al. 2007, Kopell, Boergers et al. 2010). In such models, fast excitation and delayed feedback inhibition alternate, and with appropriate strength of excitation and inhibition, oscillatory behavior occurs. When the gamma activity produced by the E-I or I-I models is periodically modulated by a theta rhythm imposed by either an external source or theta resonant cells within the network (White, Banks et al. 2000), a theta-gamma PAC is produced. Recently, the generation of theta-gamma PAC was studied (Onslow, Jones et al. 2014) using a neural mass model (NMM) proposed by Wilson and Cowan (Wilson and Cowan 1972). In NMMs, spatially averaged magnitudes are assumed to characterize the collective behavior of populations of neurons of a given type instead of modeling single cells and their interactions in a realistic network (Wilson and Cowan 1972, Jansen and Rit 1995). Specifically, the Wilson and Cowan model consists of excitatory and inhibitory neural populations which are mutually connected.

While the models mentioned above have improved our understanding of the physiological mechanism that gives rise to theta-gamma PAC, we lack modeling insights into the generation of PAC involving other frequency pairs (Sotero 2015). This is critical because experimental studies have shown that the PAC phenomenon is not restricted to either the hippocampus or to theta-gamma interactions. In fact, PAC has been detected in pairs involving all possible combinations of low and high frequencies: delta-theta (Lakatos, Shah et al. 2005), delta-alpha (Cohen, Elger et al. 2009, Ito, Maldonado et al. 2013), delta-beta (Cohen, Elger et al. 2009, Nakatani, Raffone et al. 2014), delta-gamma (Gross, Hoogenboom et al. 2013, Lee and Jeong 2013, Nakatani, Raffone et al. 2014, Szczepanski, Crone et al. 2014, Florin and Baillet 2015), theta-alpha (Cohen, Elger et al. 2009), theta-beta (Cohen, Elger et al. 2009, Nakatani, Raffone et al. 2014), theta-gamma (Lakatos, Shah et al. 2005, Demiralp, Bayraktaroglu et al. 2007, Wang, Li et al. 2011, Durschmid, Zaehle et al. 2013, Lee and Jeong 2013, McGinn and Valiante 2014, Florin and Baillet 2015), alpha-beta (Sotero, Bortel et al. 2015), alpha-gamma (Osipova, Hermes et al. 2008, Voytek, Canolty et al. 2010, Spaak, Bonnefond et al. 2012, Wang, Saalmann et al. 2012), and beta-gamma (Wang, Saalmann et al. 2012, de Hemptinne, Ryapolova-Webb et al. 2013). Furthermore, although experimental studies usually focus on one or two PAC combinations, most of the combinations mentioned above can be detected in a single experiment (Sotero, Bortel et al. 2015). This suggests a diversity and complexity of the PAC phenomenon that has not been incorporated into current computational models. Similarly, there is a need for further improvement in the mathematical methods used to detect PAC. Although a large number of methods have been proposed (Penny, Duzel et al. 2008, Tort, Komorowski et al. 2010), no gold standard has emerged.

In this work, we propose a neural mass model of a cortical column that comprises 4 cortical layers and 14 neuronal populations and study the simultaneous generation of all PAC combinations mentioned above. To estimate PAC we use a measure of the information transfer from the phase of the low frequency rhythm to the amplitude of the higher frequency oscillation, which is known as conditional transfer entropy (cTE) (Lizier, Heinzle et al. 2011). This multivariate approach provides information about the directionality of the interactions, thus distinguishing PAC from the information transfer from the amplitude to the phases (i.e. amplitude-phase coupling, or APC) which has been experimentally detected (Jiang, Bahramisharif et al. 2015). This done in contrast to previous methods which were either based on pairwise correlations between the selected phase and amplitude (Canolty, Edwards et al. 2006, Penny, Duzel et al. 2008), or provided directionality using pairwise approaches (Jiang, Bahramisharif et al. 2015), or were multivariate but did not provide directionality (Canolty, Cadieu et al. 2012). By estimating cTE from phases to amplitudes, we obtain a clearer view of the mechanisms underlying the generation of PAC in the cortical column which allows us to study the link between anatomical and effective PAC structure. In the examples shown in this paper, the neuronal populations modeled have natural frequencies in the theta, alpha and gamma bands. However, due to the effective connectivity between populations, oscillations in the delta and beta bands appear and result in PAC involving these frequencies. We focused on three combinations (delta-gamma, theta-gamma, and alpha-gamma) and explored how changes in model parameters such as the strength of the connections, time constants or external inputs strengthen or weaken the PAC phenomenon. We found that more than 60% of the obtained PAC interactions result from indirect connections and that, on average, these interactions have the same strength as direct (anatomical) connections. The cortical column circuit was analyzed as a

complex network and three different local topological measures were computed: the clustering coefficient (C_m), the efficiency (E_m) and betweenness centrality (B_m) which quantify how efficiently the information is transmitted within the network. According to our results, neuronal populations sending direct PAC connections had higher local C_m, E_m, and B_m coefficients, than populations receiving the PAC connection and populations not involved in PAC interactions. This suggests that the topology of cortical circuits plays a central role in the generation of the PAC phenomenon.

Finally, although this paper focuses on the PAC phenomenon, in order to study the generation of indirect PAC connections we also estimated other types of cross-frequency coupling such as APC, amplitude-amplitude coupling (AAC), and phase-phase coupling (PPC), as well as interactions within the same frequency band (or same-frequency coupling, SFC), and used these as predictors of indirect PAC in a linear regression analysis. We demonstrated that indirect PAC connections can be predicted by a cascade of direct CFC and SFC interactions, suggesting that PAC analysis of experimental data should be accompanied by the estimation of other types of interactions for an integrative understanding of the phenomenon.

A list of the abbreviations used in this paper is presented in Table 1.

2. Methods

2.1. A neural mass model of a cortical column

Figure 1 shows the proposed model obtained by distributing four cell classes in four cortical layers (L2/3, L4, L5, and L6). This produced 14 different neuronal populations, since not all cell types are present in each layer (Neymotin, Jacobs et al. 2011). Excitatory neurons were either regular spiking (RS) or intrinsically bursting (IB), and inhibitory neurons were either fast-spiking

(FS), or low-threshold spiking (LTS) neurons. The evolution of each population dynamics rests on two mathematical operations. Post-synaptic potentials (PSP) at the axonal hillock were converted into an average firing rate using the sigmoid function:

$$S(x) = \frac{e_0}{1+e^{r(v_0-x)}} \quad (1)$$

where the variable x represents the PSP and parameters e_0, v_0 and r represent the maximal firing rate, the PSP corresponding to the maximal firing rate e_0, and the steepness of the sigmoid function, respectively. The second operation was the conversion of firing rate at the soma and dendrites into PSP, which was done by means of a linear convolution with an impulse response $g(t)$ given by:

$$g(t) = Gkte^{-kt} \quad (2)$$

where G controls the maximum amplitude of PSP and k is the sum of the reciprocal of the average time constant (Jansen and Rit 1995). The convolution model with impulse response (2) can be transformed into a second order differential equation (Jansen and Rit 1995, Sotero, Trujillo-Barreto et al. 2007). The temporal dynamics of the average PSP in each neuronal population x_m can then be obtained by solving a system of 14 second order differential equations:

$$\frac{d^2x_m(t)}{dt^2} = -2k_m b_m \frac{dx_m(t)}{dt} - k_m^2 x_m(t) + G_m k_m \left(p_m + \sum_{n=1}^{14} \Gamma_{nm} S\left(x_n(t)\right)\right) \quad (3)$$

where n = 1,…,14 and m = 1,…,14. The populations are numbered from 1 to 14 following the order: [L2RS, L2IB, L2LTS, L2FS, L4RS, L4LTS, L4FS, L5RS, L5IB, L5LTS, L5FS, L6RS, L6LTS, L6FS]. Notice that layer 2/3 was simply labelled as L2. As can be seen in (3), neuronal populations interact via the connectivity matrix Γ_{nm}. This is an 'anatomically constrained' effective connectivity matrix (Sotero, Bortel et al. 2010) in the sense that its elements represent anatomical (i.e., direct) connections, but their strength (except the ones set to zero) can vary with

a condition or task. Inputs from neighboring columns are accounted for via p_m , which can be any arbitrary function, including white noise (Jansen and Rit 1995). Thus, equation (3) represents a system of 14 random differential equations (Carbonell, Jimenez et al. 2005).

The 'damping' parameter b_m critically determines the behavior of the system. If the connections between the populations are set to zero ($\Gamma_{nm} = 0, n \neq m$), then for $b_m > 1$ (overdamped oscillator) and $b_m = 1$ (critically damped oscillator), each neuronal population will evolve to a fixed point $\left(\frac{dx_m(t)}{dt} = 0\right)$ without oscillating. If $b_m < 1$ (underdamped oscillator), each population is capable of producing oscillations even if the inter-population coupling is set to zero. The case $b_m = 1$ corresponds to the Jansen and Rit model (Jansen and Rit 1995), which has been extensively used in the literature (David and Friston 2003, Grimbert and Faugeras 2006, Zavaglia, Astolfi et al. 2006, Sotero, Trujillo-Barreto et al. 2007, Sotero and Trujillo-Barreto 2008, Valdes-Sosa, Sanchez-Bornot et al. 2009, Ursino, Cona et al. 2010, Zavaglia, Cona et al. 2010). Thus, in this model, an individual population is not capable of oscillating, and the balance between excitation and inhibition is what produces oscillatory behavior that mimics observed Electroencephalography (EEG) signals. It should be noted that realistic models of a single inhibitory neural population are able to produce oscillations (Wang and Buzsaki 1996), but that excitatory populations were believed to only produce unstructured population bursts (Buzsáki 2006). This view has been challenged recently by both experimental and computational studies (Allene, Cattani et al. 2008, Tattini, Olmi et al. 2012). To account for the possibility of oscillatory activity in single populations, we introduced the parameter b_m with values $b_m < 1$. Tables 1 and 2 present the parameters of the model and their interpretation. As shown in table 2, FS populations have the fastest time constants, followed by IB, RS, and LTS, in that order.

208 **Table 1**. List of abbreviations.

Abbreviation	Meaning
AAC	Amplitude-amplitude coupling
APC	Amplitude-phase coupling
CFC	Cross-frequency coupling
cMI	Conditional mutual information
cTE	Conditional transfer entropy
ECoG	Electrocorticography
EEG	Electroencephalography
ESC	Envelope-to-signal correlation
FS	Fast-spiking
IB	Intrinsically bursting
LFP	Local field potential
LTS	Low-threshold
Midx	Modulation index
NMM	Neural mass model
PAC	Phase-amplitude coupling
PFC	Phase-frequency coupling
PPC	Phase-phase coupling
PSP	Postsynaptic potential
RS	Regular spiking
SFC	Same-frequency coupling

209
210

211 **Table 2.** Values and physiological interpretations of model parameters for the 14 neuronal

212 populations.

Parameter (units)	Interpretation	Value	Reference
$G(mV)$	Gain	$G_1 = 3.25$, $G_2 = 3.25$, $G_3 = 30$, $G_4 = 10$, $G_5 = 3.25$, $G_6 = 30$, $G_7 = 10$, $G_8 = 3.25$, $G_9 = 3.25$, $G_{10} = 30$, $G_{11} = 10$, $G_{12} = 3.25$, $G_{13} = 30$, $G_{14} = 10$	(Jansen and Rit 1995, Wendling, Bellanger et al. 2000, Zavaglia, Astolfi et al. 2006)
$k(s^{-1})$	Reciprocal of time constant	$k_1 = 60$, $k_2 = 70$, $k_3 = 30$, $k_4 = 350$, $k_5 = 60$, $k_6 = 30$, $k_7 = 350$, $k_8 = 60$, $k_9 = 70$, $k = 30$, $k_{11} = 350$, $k_{12} = 60$, $k_{13} = 30$, $k_{14} = 350$	(Jansen and Rit 1995, Wendling, Bellanger et al. 2000, Zavaglia, Astolfi et al. 2006)
p	External input	$p_i = 0$ for $i \neq \{5,7\}$, $p_5 = 500$, $p_7 = 150$	-

b	Damping coefficient	$b = 0.001$ for all populations	-
$e_0(s^{-1})$	Maximum firing rate	$e_0 = 5$ for all populations	(Jansen and Rit 1995)
$v_0(mV)$	Position of the sigmoid function	$v_0 = 6$ for all populations	(Jansen and Rit 1995)
$r(mV^{-1})$	Steepness of the sigmoid function	$r = 0.56$ for all populations	(Jansen and Rit 1995)

Table 3. Standard values of the anatomically constrained effective connectivity matrix Γ_{nm} (Figure 1B). All values represent anatomical (direct) connections. Nonzero values were manually tuned to produce peaks in the spectrum of $x_m(t)$ in all frequencies of interest (from delta to gamma) as well as an average LFP spectrum (Figure 6) consistent with experimental results (Maier, Adams et al. 2010, Buffalo, Fries et al. 2011). Values that are zero were taken from the literature (Neymotin, Jacobs et al. 2011).

From ↓ To →		L2/3				L4			L5				L6		
		RS	**IB**	**LTS**	**FS**	**RS**	**LTS**	**FS**	**RS**	**IB**	**LTS**	**FS**	**RS**	**LTS**	**FS**
L2/3	**RS**	19.23	12.53	34.17	14.07	1.61	0	0	3.82	1.61	0	0	0	0	0
	IB	12.53	12.53	27.47	14.07	1.61	0	0	3.82	1.61	0	0	0	0	0
	LTS	-23.45	-23.45	-52.93	-6.70	0	0	0	-23.45	-33.50	0	-16.75	-16.75	0	-11.39
	FS	-3.35	-5.36	-6.03	-20.1	0	0	0	-3.35	-6.70	0	-2.01	-3.35	0	-2.01
L4	**RS**	9.72	0	0	0	22.98	34.17	58.96	7.77	8.17	0	0	2.14	0	0
	LTS	0	0	0	0	-23.45	-52.93	-8.71	0	0	0	0	0	0	0
	FS	0	0	0	0	-6.03	-6.03	-61.64	0	0	0	0	0	0	0
L5	**RS**	1.47	0	0	0	0.47	0	0	32.89	5.36	20.77	8.71	2.14	0	0
	IB	1.21	0	0	0	0.47	0	0	1.14	46.90	20.77	8.71	4.69	0	0
	LTS	-23.45	0	0	0	0	0	0	-23.45	-23.45	-52.93	-2.01	-16.75	0	-5.36
	FS	0	0	0	0	0	0	0	-2.68	-2.68	-2.68	-61.64	0	0	0
L6	**RS**	0	0	0	0	0	0	0	0.40	1.88	0	0	48.78	34.17	15.41
	LTS	-23.45	0	0	0	0	0	0	-16.75	-16.75	0	-5.36	-23.45	-66.33	-8.71
	FS	0	0	0	0	0	0	0	0	0	0	0	-9.38	-29.48	-28.14

2.2. Estimation of phase-amplitude coupling

Several mathematical methods for detecting PAC have been proposed (Penny, Duzel et al. 2008, Canolty and Knight 2010, Tort, Komorowski et al. 2010, Canolty, Cadieu et al. 2012, Jiang, Bahramisharif et al. 2015), although each yields advantages and caveats, such that no gold

standard for the detection of PAC has emerged. Although diverse, the basis for these methods is to test the correlation between the instantaneous phase of a lower frequency rhythm and the instantaneous amplitude of the higher frequency rhythm. To compute any one of these measures, signals generated with the model (3) need to be band-pass filtered into different frequency bands. In this paper we use the following bands: delta (0.1–4 Hz), theta (4–8 Hz), alpha (8–12 Hz), beta (12–30 Hz), and gamma (30–120 Hz). To this end, we designed FIR filters using MATLAB's signal processing toolbox function *firls.m*. To remove any phase distortion, the filters were applied to the original time series in the forward and then the reverse direction using MATLAB's function *filtfilt.m* (Penny, Duzel et al. 2008). The analytic representation $y_{mk}(t)$ of each filtered signal x_{mk} (where m = 1,..,5 stands for the index of the frequency band, and k = 1,..,14, indexes the neuronal populations) was obtained using the Hilbert transform $\mathrm{Hilbert}\big(x_{mk}(t)\big)$:

$$y_{mk}(t) = x_{mk}(t) + i\mathrm{Hilbert}\big(x_{mk}(t)\big) = a_{mk}(t)e^{i\varphi_{mk}(t)} \quad (4)$$

where $a_{mk}(t)$ and $\varphi_{mk}(t)$ are the instantaneous amplitudes and phases, and i is the imaginary number. Amplitudes were normalized by subtracting the temporal mean and dividing the result by the temporal standard deviation to create the set of normalized band-passed signals. Normalization was done to facilitate comparison between different frequency bands.

Two examples of PAC measures frequently used in the literature are the modulation index (Midx) (Canolty, Edwards et al. 2006) and the envelope-to-signal correlation (ESC) (Penny, Duzel et al. 2008):

$$Midx = \left|\sum_t a_{nl}(t)e^{i\varphi_{mk}(t)}\right| \quad (5)$$

$$ESC = corr\big(\cos\big(\varphi_{mk}(t)\big), a_{nl}(t)\big) \quad (6)$$

where subindexes m and n corresponds to different frequency bands and subindexes k and l correspond to different neuronal populations. However, ESC and Midx are pairwise measures of

the correlation between phases and amplitudes and thus cannot detect directionality in the interaction. Measures such as cTE (Lizier, Heinzle et al. 2011) which are based on the information transmitted between signals should provide a clearer picture of the mechanisms generating PAC than correlation-based measures. cTE can be computed using the conditional mutual information (cMI) measure (MacKay 2003). First, we define the cMI between the phase φ_{mk} and the amplitude a_{nl} , given all the other phases (Φ) and amplitudes (A) as:

$$cMI(\varphi_{mk}, a_{nl}|\mathrm{M}) = H(\varphi_{mk}, |\mathrm{M}) - H(\varphi_{mk}, |a_{nl}, \mathrm{M}) \quad (7)$$

where $M = [\Phi,\ \mathrm{A}]$ is a matrix comprising all phases and amplitudes in all populations, except φ_{mk} and a_{nl}, and the two terms at the right side of the equation are conditional entropies (MacKay 2003). To compute cMI we use a toolbox (http://www.cs.man.ac.uk/~pococka4/MIToolbox.html) which computes several information measures using the conditional likelihood maximization algorithm (Brown, Pocock et al. 2012). cMI does not provide information about the directionality of the coupling between phases and amplitudes, which is a problem because both theoretical (Daffertshofer and van Wijk 2011) and experimental (Jiang, Bahramisharif et al. 2015) studies indicate the possibility of an information flow from amplitudes to phases. On the other hand, cTE provides directionality by estimating the cMI between one signal (the phase in our case) and the other signal (the amplitude) shifted δ steps into the future. In this paper, to estimate *cTE* from the phase to the amplitude (denoted as $cTE_{\varphi_{mk}\to a_{nl}}$), we compute cMI for N different δs and average the results (Palus, Komarek et al. 2001, Palus and Stefanovska 2003, Lizier, Heinzle et al. 2011) :

$$cTE_{\varphi_{mk}\to a_{nl}} = \frac{1}{N}\sum_{\delta=1}^{N} cMI\left(\varphi_{mk}, a_{nl}^{\delta}\middle|\widetilde{M}\right) \quad (8)$$

where a_{nl}^{δ} is derived from the amplitude time series a_{nl} at δ steps into the future, i.e. $a_{nl}^{\delta} = a_{nl}(t+\delta)$, and $\widetilde{M}$ is a matrix comprising all phases and amplitudes in all populations, except φ_{mk}. In this paper we use $N = 100$. Since we use a time step of 10^{-4} s in all simulations, we are averaging the *cMI* up to a period of 10 ms into the future.

A significance value can be attached to any of the above measures by means of a surrogate data approach (Canolty, Edwards et al. 2006, Penny, Duzel et al. 2008), where we offset φ_{mk} and a_{nl} by a random time lag. We can thus compute 1000 surrogate Midx, ESC, cMI and cTE values. From the surrogate dataset we first compute the mean μ and standard deviation σ, and then compute a z-score as:

$$Z_1 = \frac{cMI-\mu_1}{\sigma_1}\ , \quad Z_2 = \frac{cMI-\mu_2}{\sigma_2}\ , Z_3 = \frac{cMI-\mu_3}{\sigma_3}, \quad Z_4 = \frac{cTE-\mu_4}{\sigma_4} \tag{9}$$

The p-value that corresponds to the standard Gaussian variate is also computed. Z values satisfying $|Z| > 1.96$ are significant with $\alpha = 0.05$. Masks of zeros (for non-significant Z values) and ones (for significant Z-values) are created and multiplied to Midx, ESC, cMI, and cTE. Finally, a multiple comparison analysis based on the False Discovery Rate (Storey and Tibshirani 2003) is performed using the computed p-values.

2.3. Nonlinear correlation coefficient

Given the nonlinear nature of the PAC phenomenon, studying the link between the parameters of the model and the strength of PAC cannot be done with the Pearson correlation coefficient, which measures the linear correlation between two variables and is therefore not appropriate. Nonlinear measures are thus required. The underlying idea is that if the value of the variable X is considered as a nonlinear function of the variable Y, the value of Y given X can be predicted according to a nonlinear regression (Pereda, Quiroga et al. 2005). In this paper, we computed the nonlinear regression by fitting $y(t)$ with a Fourier series:

$$\hat{y}(t) = a_0 + \sum_{k=1}^{N} a_k sin(b_k x(t) + c_k)$$

(10)

where we used $N = 10$. The nonlinear correlation coefficient r_{nl} is then the value of the linear correlation between $y(t)$ and the predicted signal $\hat{y}(t)$.

2.4. Topological properties of the cortical column network

Complex network analysis have proven useful for studying the relationship between structure and function in brain networks (Honey, Kotter et al. 2007). In this paper we are interested in studying how the topology of the connectivity matrix Γ_{nm} influences the PAC phenomenon. Specifically, we want to answer the question of whether the populations involved in direct and indirect PAC interactions present the same topological properties. This means we need to focus on local properties of the network instead of global ones. In this paper we are going to compute three such properties: the local clustering coefficient, the local efficiency, and the local betweenness centrality, for the sending and receiving nodes involved in each direct or indirect PAC interaction.

In this section we are not going to distinguish between inhibitory and excitatory connections, and the analysis will be done to the absolute value of the connectivity matrix: $W = |\Gamma_{nm}|$.

Nodes of a network can be characterized by the structure of their local neighborhood. The concept of clustering of a network refers to the tendency to form cliques in the neighborhood of any given node (Watts and Strogatz 1998). This means that if node *m* is connected to node *n*, while at the same time node *n* is connected to node *s*, there is a high probability that node *m* is also connected to node *s*.

Let $A = \{a_{mn}\}$ be the directed adjacency matrix (Albert and Barabasi 2002) of the network ($a_{mn} = 1$ when there is a connection from *m* to *n*, $a_{mn} = 0$ otherwise). Let also d_m^{tot} be the

317 total degree of node *m*, and $d_m^{\leftrightarrow} = \sum_{m \neq n} a_{mn} a_{nm}$. The local clustering coefficient of node *m* for

318 weighted networks is (Fagiolo 2007):

319 $$C_m = \frac{\left(\widehat{W} + \widehat{W}^T\right)^3_{mm}}{2\left[d_m^{tot}\left(d_m^{tot} - 1\right) - 2d_m^{\leftrightarrow}\right]} \quad (11)$$

320 where $\widehat{W} = W^{1/3}$, and $\left(\widehat{W} + \widehat{W}^T\right)^3_{mm}$ is the *m*th element of the main diagonal of $\left(\widehat{W} + \widehat{W}^T\right)^3$.

321 The second measure we are going to compute is the local efficiency, calculated as (Latora and

322 Marchiori 2001, Rubinov and Sporns 2010):

323 $$E_m = \frac{1}{N-1} \sum_{j, j \neq m} \left(\vec{l}_{mj}\right)^{-1} \quad (12)$$

324 where $\vec{l}_{mj}$ is the shortest weighted path length from *m* to *j*. Thus, E_m is inversely related to the

325 path length, and measures how efficiently the network exchanges information on a local scale.

326 To account quantitatively for the role of nodes that can be crucial for connecting different

327 regions of the network by acting as bridges, the concept of betweenness centrality was

328 introduced (Newman, Barabási et al. 2006). The local weighted betweenness centrality of node *m*

329 is computed as (Rubinov and Sporns 2010) :

330 $$B_m = \frac{1}{(N-1)(N-2)} \sum_{\substack{h,j \\ j \neq m, h \neq m, j \neq h}} \frac{\rho_{hj}(m)}{\rho_{hj}}$$

331 (13)

332 where ρ_{hj} is the number of shortest paths between *h* and *j* that pass through *m*. A node with high

333 centrality is thus crucial to efficient communication.

334 To compute the C_m, E_m, and B_m measures we use Matlab functions provided in the brain

335 connectivity toolbox (https://sites.google.com/site/bctnet/).

336

337 ## 3. Results

338 ### 3.1. Detecting PAC: control analysis

We connected three excitatory neuronal populations, labeled 1, 2 and 3 (Figure 2A and 2B). The temporal dynamics of the three populations are described by a system of random differential equations identical to (3), but with n=1:3 and m=1:3. As shown in Figure 2A, there is no connection between populations 1 and 3 and both are driven by population 2. The parameters used in this simulation were: $G_1 = 3.25$, $G_2 = 4$, $G_2 = 3.25$, $G_3 = 4$, $k_1 = 330$, $k_2 = 30$, $k_3 = 400$. Inputs $p_1, p_2,$ and p_3 were white noise processes with mean 0 and standard deviations: $\sigma_1 = \sigma_2 = \sigma_3 = 3$. Simulated data were generated by numerically integrating system (3). To do this, the local linearization method for random systems was used (Carbonell, Jimenez et al. 2005) with an integration step of 10^{-4} s.

Figure 2C shows the temporal dynamics of the three populations and Figure 2D displays the corresponding spectral density. Population 2 oscillates at 4.40 Hz (theta band), whereas populations 1 and 3 have peaks at 50 and 57.8 Hz, respectively (gamma band). Because of the connections 2→1 and 2→3, there are peaks at 4.40 Hz in populations 1 and 3, and more importantly, there are secondary peaks at frequencies $50Hz \pm 4.40\ Hz$ and $57.8Hz \pm 4.40\ Hz$ on both sides of these main peaks. This shows that the low frequency (4.40 Hz) is modulating the higher frequencies (50 and 57.8 Hz) and that there is theta-gamma PAC. According to the connections shown in Figure 2A, phases in populations 1 and 3 cannot modulate the amplitudes in populations 3 and 1, respectively. Thus, an appropriate method to study the generation of PAC should not detect any modulation between populations 1 and 3. We found that when the sigmoid function is replaced by the linear function $S(x)=x$, no modulation is obtained (Figure 2E).

Figure 3A shows the PAC computed using the four measures presented in section 2.2. Non-significant values are plotted in white. The four methods correctly detect that there is no PAC involving amplitudes in the gamma band in population 2 (there is no significant spectral peak at

the gamma band, only white noise). However, according to ESC and Midx, there is significant PAC between the phases of the theta band in neuronal population 1 and the amplitudes of the gamma band in neuronal population 3, as well as PAC between the phases of the theta band in neuronal population 3 and the amplitudes of the gamma band in neuronal population 1. These results are expected because the signals in populations 1 and 3 are correlated, despite the fact that there is no connection between these populations. Regardless, cMI and cTE distinguished the correct effective interactions between the three populations.

There are cases where cMI fails to estimate the correct connections. For instance, Figure 3B shows the results of increasing the noise ($\sigma_1 = \sigma_2 = \sigma_3 = 10$), which caused the measures ESC, Midx and cMI to yield similar results and estimate a significant effective connection between populations 1 and 3 that did not exist. Regardless, cTE was still able to distinguish the correct pattern of connections despite the increase in the noise level. When we further increased the noise ($\sigma_1 = \sigma_2 = \sigma_3 = 30$), no significant results were obtained for any of the four measures (not shown in the figure).

3.2. Generation of multiple PAC combinations

In this section, we study the generation of PAC in the cortical column circuit depicted in Figure 1. Since we are interested in the interaction between the rhythms produced by the nonlinear dynamics of the neuronal populations (not their correlation) and in the directionality of that interaction (from phases to amplitudes), we only compute cTE.

The values of the parameters used are shown in tables 2 and 3. White noise with a mean of zero and standard deviation $\sigma = 1$ was added to the external inputs. Five seconds of data were simulated and the first two seconds were discarded to avoid transient behavior. Thus, subsequent steps were carried out with the remaining three seconds.

Figure 4 presents the temporal evolution of the average PSP in each neuronal population. Time series coloured in red correspond to excitatory populations (L2RS, L2IB, L4RS, L5RS, L5IB, L6RS), whereas inhibitory populations (L2LTS, L4LTS, L5LTS, L6LTS) are represented in green. As seen in the figure, the generated signals show the characteristic 'waxing and waning' (i.e, amplitude modulation) observed in real EEG signals.

Figure 5 presents the normalized spectrum of the signals displayed in Figure 4. Excitatory populations are depicted in red and inhibitory populations are depicted in green. The six excitatory populations have their main spectrum peak in the alpha band, but they also present energy in the delta and theta bands. Slow inhibitory populations have the highest peak in the theta band, but also have energy in delta, alpha bands. Fast inhibitory populations were set to yield a peak in the gamma band, but due to the interaction with other populations they yield significant peaks in other frequencies as well, especially in the theta and alpha bands. This is evident when compared to the spectrum (in black) of the population when interactions between different populations are set to zero ($\Gamma_{nm} = 0, n \neq m$). Peaks in black correspond to the natural frequency of oscillation for the populations L2RS (9.00 Hz), L2IB (10.67 Hz), L2LTS (7.00 Hz), L2FS (58.67 Hz), L4RS (9.33 Hz), L4LTS (7.00 Hz), L4FS (87.00 Hz), L5RS (8.67 Hz), L5IB (9.67 Hz), L5LTS (7.00 Hz), L5FS (63.99 Hz), L6RS (7.67 Hz), L6LTS (7.33 Hz), and L6FS (59.67 Hz).

To compare our simulated data with actual local field potential (LFP) data, we computed an approximation of the average LFP as the difference between the sum of excitatory and inhibitory activities in each layer.

Figure 6A displays the temporal dynamics of the LFP in each cortical layer and Figure 6B shows the corresponding spectral density. Thus, parameter values presented in tables 2 and 3 result in

low frequency oscillations (delta, theta and alpha) with highest power in layers 5 and 6 while gamma oscillations have its main power in layer 2/3. This is in agreement with recent findings suggesting that gamma activity is predominant in superficial layers while lower frequencies are predominant in deep layers (Maier, Adams et al. 2010, Buffalo, Fries et al. 2011).

To test the existence of PAC, we filtered each time series in Figure 4 into five frequency bands from delta to gamma (see section 2.2) and applied the Hilbert transform to obtain instantaneous phases and amplitudes for each frequency band and each neuronal population.

Ten different PAC combinations between a low-frequency phase and a higher-frequency amplitude were computed using the cTE measure: delta-theta, delta-alpha, delta-beta, delta-gamma, theta-alpha, theta-beta, theta-gamma, alpha-beta, alpha-gamma, and beta-gamma. Each PAC combination consisted of a matrix of 14x14 cTE values representing all possible interactions between the 14 neuronal populations. To test the significance of these values, surrogate data was computed, followed by a multiple comparison analysis as described in section 2.2.

Results include nine out of the ten PAC combinations (Figure 7). The delta-beta PAC combination was not included since no significant values were obtained for the set of parameters used.

The strongest PAC value found was between the phase of the alpha band in L2IB and the amplitude of the gamma band in L4FS, which we will denote as L2IB→ L4FS. Other strong values found were theta-gamma (L6RS→L4FS, L4RS→L4FS, L2IB→L4FS, L6RS→L5FS), and alpha-gamma (L2IB→L5FS, L4FS→L4FS, L2FS→L4FS). Some of these values do not represent direct connections between the populations. For example, the strongest causal connection (L2IB→ L4FS) does not correspond to an anatomical (direct) connection (see Figure

1). Thus, we emphasize that PAC matrices (Figure 7) represent effective connections, which can correspond or not correspond with anatomical connections. To make this clearer, anatomical connections in Figure 7 are represented with black dots.

3.3. Parameter sensitivity analysis

Some of the parameters presented in table 2 were taken from the neural mass literature (Jansen and Rit 1995, Wendling, Bellanger et al. 2000), and parameters with no equivalent in the literature were assigned physiologically reasonable values. Thus, it is necessary to explore how changes in these parameters can affect PAC values. In this section, for the sake of simplicity, we focus on three PAC combinations which involve the gamma rhythm and have been of great interest in the literature: delta-gamma, theta-gamma, and alpha-gamma.

3.3.1 Controlling the strength of PAC

We selected nine different parameters and explored how their change affected the strength of the PAC phenomenon. For each parameter we considered 100 different values and thus performed 100 different simulations. The parameters were: 1) a multiplying factor $\eta = 0.3{:}\,0.3{:}\,3$ controlling the global strength of the connectivity matrix ($\Gamma_{nm} = \eta\Gamma_{nm}$) , 2) the reciprocal of the time constant of RS populations ($k_{RS} = 5{:}\,5{:}\,500s^{-1}$), 3) the reciprocal of the time constant of IB populations ($k_{IB} = 5{:}\,5{:}\,500s^{-1}$), 4) the reciprocal of the time constant of LTS populations ($k_{LTS} = 5{:}\,5{:}\,500s^{-1}$), 5) the reciprocal of the time constant of FS populations ($k_{FS} = 5{:}\,5{:}\,500s^{-1}$), 6) the external input to the L4RS population ($p_5 = 10{:}\,10{:}\,1000$), 7) the external input to the L4FS population ($p_7 = 10{:}\,10{:}\,1000$), 8) the gains of the six excitatory populations ($G_E \equiv G_1 = G_2 = G_5 = G_8 = G_9 = G_{12} = 0.2{:}\,0.2{:}\,20$), and 9) the gains of the eight inhibitory populations ($G_I \equiv G_3 = G_4 = G_6 = G_7 = G_{10} = G_{11} = G_{13} = G_{14} = 0.3{:}\,0.3{:}\,30$).

Then, for each PAC combination we obtained 14x14x100= 19600 cTE values (although many of them are zero). We summarized that information by taking the strongest value found in each simulation, which results in a series of 100 values for each PAC combination. Figure 8A displays the mean and standard deviation of the 100-point series of the strongest PAC values for the three PAC combinations considered. In the figure, Delta-gamma PAC is depicted in orange, theta-gamma PAC in green, and alpha-gamma PAC in blue. Our results shows that for the three PAC combinations, the highest increase in cTE was obtained when changing the reciprocal time constants of LTS populations.

The exploration of the parameter space is important because PAC has been suggested to be the carrier mechanism for the interaction of local and global processes in the brain, and is thus directly related to the integration of distributed information in the brain (Canolty and Knight 2010). Neuronal circuits can thus control the amount of information transmitted in the PAC phenomenon by changing the values of physiological parameters of specific populations.

3.3.2 On the influence of the connectivity matrix Γ_{nm} on PAC strength

An important problem in neuroscience is the link between structural and functional brain networks (Honey, Sporns et al. 2009, Stam, van Straaten et al. 2015). In the context of this work, it is of interest to study the influence of the connectivity matrix Γ_{nm} on the generated PAC phenomenon.

For each of the 100 simulations we also computed the fraction (ξ) of PAC connections that corresponded to anatomical connections. The obtained ratios for delta-gamma, theta-gamma, and alpha-gamma, were 0.45 ± 0.12, 0.36 ± 0.04, and 0.35 ± 0.04, respectively. Figure 8B shows the plot of the ratios ξ versus the factor η, and the corresponding linear model fit. The linear

correlation values (r_l) between ξ and η for delta-gamma, theta-gamma, and alpha-gamma PAC were 0.17, 0.08, and 0.15, respectively. The values were significant with $\alpha = 0.05$.

Figure 8C displays the series of 100 PAC values versus η. The solid line corresponds to the fit of a linear model. The linear correlation values between delta-gamma, theta-gamma, alpha-gamma and η were 0.16, 0.13, and 0.11, respectively. As expected, the linear correlation between the strength of the PAC phenomenon and the global strength of the connectivity matrix Γ_{nm} was weak, although significant (with $\alpha = 0.05$). We then performed a nonlinear regression analysis (equation 10) with η as the regressor and computed the nonlinear correlation coefficient (section 2.3). The nonlinear correlation values between delta-gamma, theta-gamma, alpha-gamma and η were 0.44, 0.53, and 0.58, respectively, showing that there is a strong nonlinear relationship between the strength of PAC and effective connectivity between the populations involved. The values were significant as tested with the surrogate data approach (section 2.2).

We also counted all significant PAC connections obtained in the 100 simulations. The vectors of significant connections for delta-gamma, theta-gamma, and alpha-gamma PAC comprised 595, 1464, and 1499, cTE values, respectively, for the PAC interactions that have a corresponding anatomical connection (direct interactions), and 740, 2656, and 2788 for the interactions without an anatomical equivalent (indirect interactions). The mean and standard deviations of these connections are presented in Figure 8D. Our results showed that for the three PAC combinations, the average strength of direct PAC interactions was slightly higher than indirect PAC interactions, but this difference was not statistically significant (as tested with a t-test, $p<0.05$).

Finally, we computed three local topological measures (section 2.4) for the network of 14 coupled neuronal populations (Fig 1A): C_m, E_m, and B_m. The edges of the network were the absolute values of the connections between the populations (Figure 1B). We found that on

498 average, indirect PAC interactions are made by populations with higher C_m (Figure 9A), E_m
499 (Figure 9B), and B_m (Figure 9C) than populations making direct connections, and populations
500 not involved in PAC connections. Populations receiving indirect PAC connections had also on
501 average higher topological measures than populations receiving direct interactions.

502 **3.4. Generation of other types of CFC**

503 The neural mass model presented in this paper can generate rich temporal dynamics. Studies of
504 the dynamics generated by the Jansen and Rit model, which is the basis for our model, can be
505 found elsewhere (Grimbert and Faugeras 2006, Faugeras, Veltz et al. 2009, Spiegler, Kiebel et
506 al. 2010). In this paper we focused on PAC, but this is only one type of the general phenomenon
507 of CFC which results from nonlinearities in brain dynamics. It is thus not unexpected to find
508 other types of CFC in the signals generated by our model (for example, the temporal dynamics of
509 L5RS in Figure 4 correspond to frequency modulation). In addition to PAC, other types of CFC
510 such as AAC, PPC, and phase-frequency coupling (PFC) have been explored in the literature
511 (Jirsa and Muller 2013, Hyafil, Giraud et al. 2015) and could all be calculated using equation (8)
512 after replacing $a_{nl}(t)$ and $\varphi_{mk}(t)$ with the appropriate time series.
513 Recently, the analysis of resting state electrocorticography (ECoG) data revealed that the
514 amplitude of gamma oscillations can drive the phase of alpha oscillations, i.e, APC (Jiang,
515 Bahramisharif et al. 2015). Although this experimental result may seem surprising, it is consistent
516 with theoretical results in the NMM literature. Specifically, starting with a network of Wilson and
517 Cowan oscillators, equations for the instantaneous phases were obtained which depended on the
518 instantaneous amplitudes of the oscillators in the network (Daffertshofer and van Wijk 2011).
519 Thus, by setting different natural frequencies for the oscillators in the network, it is possible to
520 obtain not only PAC but other types of CFC. To test the existence of APC we computed:

$$cTE_{a_{nl}\to\varphi_{mk}} = \frac{1}{N}\sum_{\delta=1}^{N} cMI\left(a_{nl}, \varphi_{mk}^{\delta} \middle| \widetilde{M}\right) \quad (14)$$

where φ_{mk}^{δ} is derived from the phase time series φ_{mk} at δ steps into the future, i.e. $\varphi_{mk}^{\delta} = \varphi_{mk}(t+\delta)$, and $\widetilde{M}$ is a matrix comprising all phases and amplitudes in all populations, except a_{nl}. Figure 10 shows the APC estimated from the simulated data shown in Figures 4 and 5, with the strongest values corresponding to the gamma-delta and gamma-theta APC combinations. Our simulation supports the existence of APC as recently proposed (Jiang, Bahramisharif et al. 2015).

3.5. Mechanisms mediating indirect PAC interactions

Due to the prevalence of indirect PAC interactions (Figure 7) it is necessary to investigate the mechanisms generating them. As mentioned in section 3.4, theoretical results have shown that amplitudes and phases are coupled even under weak coupling (Guckenheimer and Holmes 1997, Daffertshofer and van Wijk 2011). Thus, we expect that indirect information transfer from the phase of one population to the amplitude of the receiving population is mediated by direct interactions between phases and amplitudes via the connectivity matrix Γ_{nm}. It should be noted that although PAC typically refers to the interaction between the phase of a low frequency rhythm and the amplitude of a higher frequency rhythm, interactions between phases and amplitudes of the same frequency or between the phase of a high frequency and the amplitude of a low frequency are also possible.

In this section, to explore the mechanism mediating indirect PAC interactions, we focused on three populations labelled from 1 to 3 (Figures 11 and 12) and connected in such a way that there was not a direct connection between populations 1 and 3:1→2→3. Population 1 oscillated in the theta band and population 3 oscillated in the gamma band. Two different cases were considered for population 2. Case I (Figure 11): Population 2 oscillated with a frequency lower (delta band)

than population 1, and Case II (Figure 12): population 2 oscillated with a frequency higher (beta band) than population 1. Five different types of CFC were computed between the three populations (PAC, APC, PPC, AAC, and PFC) while varying the connectivity parameters between populations 1 and 2 (c_{12}) and between populations 2 and 3 (c_{23}). SFC was also considered and labelled in the same way as the CFC interactions. For example, $PPC_{\theta_1\theta_2}$, is the cTE from the phase of theta in population 1 to the phase of theta in population 2. To test the significance of these values, surrogate data was computed, followed by a multiple comparison analysis (section 2.2). As a control, we computed the cTE from populations 2 and 3 to population 1 for all possible types of interactions (such as $PPC_{\theta_2\theta_1}$), and confirmed they were not statistically significant.

There are several pathways that could transfer information from the phase of the theta oscillation in population 1 to the amplitude of the gamma oscillation in population 3 ($PAC_{\theta_1\gamma_3}$). For example, a simple model could involve $PPC_{\theta_1\theta_2}$ followed by PAC between the theta rhythm in population 2 and the gamma rhythm in population 3: $PAC_{\theta_1\gamma_3} = PPC_{\theta_1\theta_2} + PAC_{\theta_2\gamma_3}$. A more complicated one is: $PAC_{\theta_1\gamma_3} = PPC_{\theta_1\delta_2} + PPC_{\delta_2\delta_3} + PAC_{\delta_3\gamma_3}$.

To compare different models (Table 4), we fitted a linear regression to $PAC_{\theta_1\gamma_3}$ and computed the coefficient of determination (R^2) as a function of parameter c_{23}. For Case I we found that the three best models were Model 1 ($PAC_{\theta_1\gamma_3} = PPC_{\theta_1\theta_2} + PAC_{\theta_2\gamma_3}$), Model 7 ($PAC_{\theta_1\gamma_3} = PPC_{\theta_1\delta_2} + PPC_{\delta_2\delta_3} + PAC_{\delta_3\gamma_3}$), and Model 3 ($PAC_{\theta_1\gamma_3} = PPC_{\theta_1\delta_2} + PAC_{\delta_2\gamma_3}$), with Model 1 being the best model for low values of c_{23}, and Model 7 for the high values. On the other hand, we obtained the opposite behavior for Case II, i.e, Model 7 was the best model for low c_{23} values, whereas Model 1 was better at explaining $PAC_{\theta_1\gamma_3}$ for high c_{23} values. The correlation between the 16 CFC and SFC variables involved in the ten models is displayed in the last panel

for both cases (Figures 11 and 12). Although we found significant PFC combinations, models involving these combinations were very weak predictors of $PAC_{\theta_1\gamma_3}$ (with R^2 <0.08 in all cases) and were thus not included in Table 3 and Figures 11 and 12.

Table 4. Indirect PAC modeled as a cascade of direct CFC and SFC in a three population network. Two cases were considered: population 2 oscillates in the beta (β) band (Case I), and population 2 oscillates in the delta (δ) band (Case II). Populations 1 and 3 always oscillate in the theta (θ) and gamma (γ) bands, respectively.

Model	Case I	Case II
1	$PAC_{\theta_1\gamma_3} = PPC_{\theta_1\theta_2} + PAC_{\theta_2\gamma_3}$	$PAC_{\theta_1\gamma_3} = PPC_{\theta_1\theta_2} + PAC_{\theta_2\gamma_3}$
2	$PAC_{\theta_1\gamma_3} = PAC_{\theta_1\theta_2} + AAC_{\theta_2\gamma_3}$	$PAC_{\theta_1\gamma_3} = PAC_{\theta_1\theta_2} + AAC_{\theta_2\gamma_3}$
3	$PAC_{\theta_1\gamma_3} = PPC_{\theta_1\beta_2} + PAC_{\beta_2\gamma_3}$	$PAC_{\theta_1\gamma_3} = PPC_{\theta_1\delta_2} + PAC_{\delta_2\gamma_3}$
4	$PAC_{\theta_1\gamma_3} = PAC_{\theta_1\beta_2} + AAC_{\beta_2\gamma_3}$	$PAC_{\theta_1\gamma_3} = PAC_{\theta_1\delta_2} + AAC_{\delta_2\gamma_3}$
5	$PAC_{\theta_1\gamma_3} = PPC_{\theta_1\theta_2} + PPC_{\theta_2\theta_3} + PAC_{\theta_3\gamma_3}$	$PAC_{\theta_1\gamma_3} = PPC_{\theta_1\theta_2} + PPC_{\theta_2\theta_3} + PAC_{\theta_3\gamma_3}$
6	$PAC_{\theta_1\gamma_3} = PPC_{\theta_1\beta_2} + PPC_{\beta_2\theta_3} + PAC_{\theta_3\gamma_3}$	$PAC_{\theta_1\gamma_3} = PPC_{\theta_1\delta_2} + PPC_{\delta_2\theta_3} + PAC_{\theta_3\gamma_3}$
7	$PAC_{\theta_1\gamma_3} = PPC_{\theta_1\beta_2} + PPC_{\beta_2\beta_3} + PAC_{\beta_3\gamma_3}$	$PAC_{\theta_1\gamma_3} = PPC_{\theta_1\delta_2} + APC_{\delta_2\delta_3} + PAC_{\delta_3\gamma_3}$
8	$PAC_{\theta_1\gamma_3} = PAC_{\theta_1\theta_2} + APC_{\theta_2\theta_3} + PAC_{\theta_3\gamma_3}$	$PAC_{\theta_1\gamma_3} = PAC_{\theta_1\theta_2} + APC_{\theta_2\theta_3} + PAC_{\theta_3\gamma_3}$
9	$PAC_{\theta_1\gamma_3} = PAC_{\theta_1\beta_2} + APC_{\beta_2\theta_3} + PAC_{\theta_3\gamma_3}$	$PAC_{\theta_1\gamma_3} = PAC_{\theta_1\delta_2} + APC_{\delta_2\theta_3} + PAC_{\theta_3\gamma_3}$
10	$PAC_{\theta_1\gamma_3} = PAC_{\theta_1\beta_2} + APC_{\beta_2\beta_3} + PAC_{\beta_3\gamma_3}$	$PAC_{\theta_1\gamma_3} = PAC_{\theta_1\delta_2} + APC_{\delta_2\delta_3} + PAC_{\delta_3\gamma_3}$

4. Discussion

We have proposed a neural mass model that captures the phase-amplitude coupling between layers in a cortical column. The model comprises fourteen interconnected neuronal populations distributed across four cortical layers (L2/3, L4, L5 and L6). We omitted layer 1, because it does not include somas (Binzegger, Douglas et al. 2004). Based on experimental reports on the strength of the inputs to each layer (Binzegger, Douglas et al. 2004, Jellema, Brunia et al. 2004),

583 we only considered external inputs to the RS and FS populations in layer 4, thus neglecting
584 possible external inputs to other layers.
585 According to our results, the parameters with the strongest influence on the strength of PAC
586 were the time constants (especially the ones for LTS, FS, and IB populations). As expected, in
587 order to generate PAC, nonlinearities in the model are essential. As was shown in Figure 2E,
588 when the sigmoid function was substituted with a linear function, no modulation was obtained.
589 Additionally, the strength of PAC was best modeled by a nonlinear regression of the connectivity
590 values instead of a linear regression. Thus, our results show that the nonlinear interaction of
591 neuronal populations (via the sigmoid function and the connectivity matrix) can produce PAC
592 combinations with frequencies different from the natural frequencies of the oscillators involved.
593 Our model of oscillators with natural frequencies in the theta, alpha and gamma bands was able
594 to produce significant PAC involving delta and beta rhythms, including delta-alpha, delta-beta,
595 delta-gamma, theta-beta, alpha-beta, and beta-gamma. Interestingly, some peaks in the beta band
596 are harmonics of theta and alpha oscillations, such as the beta peak at 19 Hz in the spectrum of
597 L4FS in Figure 5. Due to the interaction between the populations, there is a statistically
598 significant PAC from the phase of beta in L4FS to the amplitude of gamma in L2FS, L4FS,
599 L5FS and L6FS. Note that of these PAC interactions, only L4FS→L4FS corresponds to an
600 anatomical connection (Figure 1B and table 3). If we take into account all PAC combinations in
601 Figure 7, less than 40% of all significant PAC values (60/160=37.50%) corresponded to
602 anatomical connections. This suggests that although effective connections are constrained by
603 direct (anatomical) connections (Sotero, Bortel et al. 2010) additional factors are needed to fully
604 explain the link between anatomical and effective connectivity. Interestingly, our numerical
605 simulations showed that on average the strength of the PAC phenomenon mediated by direct and

606 indirect connections is approximately the same. However, local topological measures such as
607 clustering coefficient, efficiency, and betweenness centrality were the highest for populations
608 making indirect connections when compared to populations making direct PAC connections, to
609 populations receiving PAC connections, and to populations not involved on the generation of
610 PAC. This suggest that the topology of cortical circuits shapes the generation of the PAC
611 phenomenon. This is another factor to consider when studying the origin of PAC during
612 neurodegenerative disorders known to affect both local and global brain circuitry.
613 One limitation of the present approach is that model parameters are loosely constrained from
614 existing neurophysiological data. Thus, although our model provides insight about the
615 emergence of PAC in a complex network whose spectral and connectivity properties resemble
616 that of a cortical column, specific conclusions should await to more knowledge of these data.

617 **4.1. Comparison with previous models of PAC generation**

618 The first computational models of PAC generation were realistic models of the theta-gamma
619 coupling in the hippocampus (Kopell, Boergers et al. 2010). These models considered networks
620 of hundreds of interconnected neurons which were individually modeled by either a single
621 compartment (White, Banks et al. 2000) or realistically represented by multiple compartments
622 for the soma, axon, and dendrites (Tort, Rotstein et al. 2007). A practical disadvantage of this
623 approach is that it needs high computational power, but more importantly, the use of such
624 realistic models produces hundreds or thousands of variables and parameters, making it difficult
625 to determine their influence on the generated average network characteristics. This is especially
626 critical if we are interested in analyzing the link of PAC and mesoscopic phenomena like
627 functional magnetic resonance signals (Wang, Saalmann et al. 2012). The analysis of multiple
628 PAC combinations as done in this paper would be even more difficult with realistic networks. By

629 comparison, our model of one cortical column comprised only 14 second-order (or 28 first-order)
630 differential equations, which can be easily solved using any modern personal computer.
631 Additionally, previous models of PAC generation, both the ones based on realistic networks
632 (Kopell, Boergers et al. 2010) and the ones based on neural mass models (Onslow, Jones et al.
633 2014) studied the phenomenon in a qualitative way, such that they did not actually compute a
634 PAC measure but limited their analysis to the generation of temporal dynamics resembling PAC.
635 This makes it difficult to compare their results with our quantitative approach based on
636 information theory.

637 **4.2. Indirect PAC connections can be predicted by a cascade of direct CFC and**
638 **interactions within the same frequency band**

639 As a unifying theory of EEG organization, it has been proposed that the EEG is hierarchically
640 organized such that the delta phase modulates the theta amplitude, and the theta phase modulates
641 the gamma amplitude (Lakatos, Shah et al. 2005). It was also proposed that this oscillatory
642 hierarchy controls baseline excitability and that the hierarchical organization of ambient
643 oscillatory activity allows the auditory cortex to structure its temporal activity pattern to optimize
644 the processing of rhythmic inputs. Recent findings suggest a somewhat different hierarchy of
645 oscillatory activity with regard to these frequency bands (Sotero, Bortel et al. 2015). Sotero et al.
646 did not observe PAC between the delta and theta bands in rat area S1FL: PAC was statistically
647 significant between the phases of the delta and theta bands and the amplitudes of the beta and
648 gamma bands, but not between the phase of the delta band and the amplitude of the theta band.
649 Their data support specific PAC interactions, but not a clear hierarchical PAC structure. The
650 differences between Lakatos et al.'s findings and Sotero et al.'s findings are consistent with their
651 proposal that the hierarchical structure found in the auditory cortex may support processing of

652 rhythmic auditory stimuli, which are less common in natural somatosensory stimuli to the
653 forepaw. Both studies were restricted to PAC and did not explore whether the oscillatory
654 hierarchy might involve other types of CFC. While historically PAC and PPC have been the
655 subject of most experimental and modeling studies, other types of CFC are attracting increasing
656 interest (Jirsa and Muller 2013, Hyafil, Giraud et al. 2015, Jiang, Bahramisharif et al. 2015). Our
657 results show that indirect PAC is better understood if analyzed along with direct PAC and other
658 types of direct CFC and SFC connections. Our simulations do not suggest a specific oscillatory
659 hierarchy like the one proposed by Lakatos et al., but multiple contributing cascades of CFC and
660 SFC. Future analysis of experimental data will need to determine the functional importance of
661 these different possible pathways.

662 **4.3. cTE as a unified approach to estimate CFC**

663 In this work, we used the average cTE, computed using the conditional mutual information
664 (Palus, Komarek et al. 2001, Palus and Stefanovska 2003) to measure the influence of the phase
665 of a low frequency rhythm on the amplitude of a higher frequency rhythm, and used it as an index
666 of PAC. A known limitation of the cTE approach is that it requires long time series (Hlavackova-
667 Schindler, Palus et al. 2007). For this reason, we used time series comprising of 30,000 time
668 instants. Recent studies have shown that cTE is biased as its values depend on the
669 autodependency coefficient in a dynamical system (Runge, Heitzig et al. 2012). Conditional TE
670 was chosen over pairwise mutual information (MacKay 2003) or the pairwise information flow
671 (Liang 2014) because pairwise analysis cannot distinguish between connectivity configurations
672 such as [X→Y, X→Z, Z→Y] and [X→Z, Z→Y] (Ding 2006).
673 An advantage of measures based on information theory is that they are model-free. This is in
674 contrast to other measures like Granger causality, which are based on autoregressive models

675 (Seth, Barrett et al. 2015). Furthermore, Granger causality should not be applied to band-passed
676 signals because the filtering process produces a large increase in the empirical model order,
677 which often results in spurious results (Barnett and Seth 2011). Another advantage of the cTE
678 measure is that it can be used to estimate any type of CFC, not just PAC. Thus, it provides a
679 unified measure to study the CFC phenomenon.
680 cTE has often been given a causal interpretation, however a more recent point of view (Lizier
681 and Prokopenko 2010) suggests that cTE should be interpreted as predictive information transfer,
682 i.e. the amount of information that a source variable adds to the next state of the destination
683 variable. Ultimately, interventions are required to detect causal interactions (Pearl 2000). This
684 formalism is used in a causal measure called information flow (Ay and Polani 2008), which is
685 also based on the cMI .
686
687
688

689 **Acknowledgements**

690 The author thanks Lazaro Sanchez for his comments on a previous version of the manuscript,
691 and Erica A. Baines for English editing. This work was partially supported by grant RGPIN-
692 2015-05966 from Natural Sciences and Engineering Research Council of Canada.
693

694 **References**

695 Albert, R. and A. L. Barabasi (2002). "Statistical mechanics of complex networks." Reviews of Modern
696 Physics **74**(1): 47-97.

697 Allene, C., A. Cattani, J. B. Ackman, P. Bonifazi, L. Aniksztejn, Y. Ben-Ari and R. Cossart (2008).
698 "Sequential generation of two distinct synapse-driven network patterns in developing neocortex." J
699 Neurosci **28**(48): 12851-12863.
700 Albert, R. and A. L. Barabasi (2002). "Statistical mechanics of complex networks." Reviews of Modern
701 Physics **74**(1): 47-97.
702 Allene, C., A. Cattani, J. B. Ackman, P. Bonifazi, L. Aniksztejn, Y. Ben-Ari and R. Cossart (2008).
703 "Sequential generation of two distinct synapse-driven network patterns in developing neocortex." J
704 Neurosci **28**(48): 12851-12863.
705 Ay, N. and D. Polani (2008). "Information flows in causal networks." Advances in Complex Systems **11**(1):
706 17-41.
707 Barnett, L. and A. K. Seth (2011). "Behaviour of Granger causality under filtering: theoretical invariance
708 and practical application." J Neurosci Methods **201**(2): 404-419.
709 Binzegger, T., R. J. Douglas and K. A. C. Martin (2004). "A quantitative map of the circuit of cat primary
710 visual cortex." Journal of Neuroscience **24**(39): 8441-8453.
711 Bragin, A., G. Jando, Z. Nadasdy, J. Hetke, K. Wise and G. Buzsaki (1995). "Gamma (40-100-Hz) Oscillation
712 in the Hippocampus of the Behaving Rat." Journal of Neuroscience **15**(1): 47-60.
713 Brown, G., A. Pocock, M. J. Zhao and M. Lujan (2012). "Conditional Likelihood Maximisation: A Unifying
714 Framework for Information Theoretic Feature Selection." Journal of Machine Learning Research **13**: 27-
715 66.
716 Buffalo, E. A., P. Fries, R. Landman, T. J. Buschman and R. Desimone (2011). "Laminar differences in
717 gamma and alpha coherence in the ventral stream." Proc Natl Acad Sci U S A **108**(27): 11262-11267.
718 Buzsáki, G. (2006). Rhythms of the brain. Oxford ; New York, Oxford University Press.
719 Canolty, R. T., C. F. Cadieu, K. Koepsell, R. T. Knight and J. M. Carmena (2012). "Multivariate phase-
720 amplitude cross-frequency coupling in neurophysiological signals." IEEE Trans Biomed Eng **59**(1): 8-11.

721 Canolty, R. T., E. Edwards, S. S. Dalal, M. Soltani, S. S. Nagarajan, H. E. Kirsch, M. S. Berger, N. M. Barbaro
722 and R. T. Knight (2006). "High gamma power is phase-locked to theta oscillations in human neocortex."
723 Science **313**(5793): 1626-1628.
724 Canolty, R. T. and R. T. Knight (2010). "The functional role of cross-frequency coupling." Trends Cogn Sci
725 **14**(11): 506-515.
726 Carbonell, F., J. C. Jimenez, R. J. Biscay and H. De La Cruz (2005). "The local linearization method for
727 numerical integration of random differential equations." Bit Numerical Mathematics **45**(1): 1-14.
728 Cohen, M. X., C. E. Elger and J. Fell (2009). "Oscillatory activity and phase-amplitude coupling in the
729 human medial frontal cortex during decision making." J Cogn Neurosci **21**(2): 390-402.
730 Daffertshofer, A. and B. C. van Wijk (2011). "On the Influence of Amplitude on the Connectivity between
731 Phases." Front Neuroinform **5**: 6.
732 David, O. and K. J. Friston (2003). "A neural mass model for MEG/EEG: coupling and neuronal dynamics."
733 Neuroimage **20**(3): 1743-1755.
734 de Hemptinne, C., E. S. Ryapolova-Webb, E. L. Air, P. A. Garcia, K. J. Miller, J. G. Ojemann, J. L. Ostrem, N.
735 B. Galifianakis and P. A. Starr (2013). "Exaggerated phase-amplitude coupling in the primary motor
736 cortex in Parkinson disease." Proc Natl Acad Sci U S A **110**(12): 4780-4785.
737 Demiralp, T., Z. Bayraktaroglu, D. Lenz, S. Junge, N. A. Busch, B. Maess, M. Ergen and C. S. Herrmann
738 (2007). "Gamma amplitudes are coupled EEG during visual to theta phase in human perception."
739 International Journal of Psychophysiology **64**(1): 24-30.
740 Ding, M., Chen, Y., Bressler, S.L (2006). Granger causality: Basic theory and application to neuroscience.
741 Handbook of Time Series Analysis. W. Schelter. S., N., & Timmer, J. , Wiley, Wienheim.
742 Durschmid, S., T. Zaehle, K. Kopitzki, J. Voges, F. C. Schmitt, H. J. Heinze, R. T. Knight and H. Hinrichs
743 (2013). "Phase-amplitude cross-frequency coupling in the human nucleus accumbens tracks action
744 monitoring during cognitive control." Front Hum Neurosci **7**: 635.

745 Fagiolo, G. (2007). "Clustering in complex directed networks." Physical Review E **76**(2).

746 Faugeras, O., R. Veltz and F. Grimbert (2009). "Persistent neural states: stationary localized activity

747 patterns in nonlinear continuous n-population, q-dimensional neural networks." Neural Comput **21**(1):

748 147-187.

749 Florin, E. and S. Baillet (2015). "The brain's resting-state activity is shaped by synchronized cross-

750 frequency coupling of neural oscillations." Neuroimage **111**: 26-35.

751 Grimbert, F. and O. Faugeras (2006). "Bifurcation analysis of Jansen's neural mass model." Neural

752 Comput **18**(12): 3052-3068.

753 Gross, J., N. Hoogenboom, G. Thut, P. Schyns, S. Panzeri, P. Belin and S. Garrod (2013). "Speech Rhythms

754 and Multiplexed Oscillatory Sensory Coding in the Human Brain." Plos Biology **11**(12).

755 Guckenheimer, J. and P. Holmes (1997). Nonlinear oscillations, dynamical systems, and bifurcations of

756 vector fields. New York, Springer.

757 Hlavackova-Schindler, K., M. Palus, M. Vejmelka and J. Bhattacharya (2007). "Causality detection based

758 on information-theoretic approaches in time series analysis." Physics Reports-Review Section of Physics

759 Letters **441**(1): 1-46.

760 Honey, C. J., R. Kotter, M. Breakspear and O. Sporns (2007). "Network structure of cerebral cortex

761 shapes functional connectivity on multiple time scales." Proc Natl Acad Sci U S A **104**(24): 10240-10245.

762 Honey, C. J., O. Sporns, L. Cammoun, X. Gigandet, J. P. Thiran, R. Meuli and P. Hagmann (2009).

763 "Predicting human resting-state functional connectivity from structural connectivity." Proc Natl Acad Sci

764 U S A **106**(6): 2035-2040.

765 Hyafil, A., A. L. Giraud, L. Fontolan and B. Gutkin (2015). "Neural Cross-Frequency Coupling: Connecting

766 Architectures, Mechanisms, and Functions." Trends Neurosci **38**(11): 725-740.

767 Ito, J., P. Maldonado and S. Grun (2013). "Cross-frequency interaction of the eye-movement related LFP

768 signals in V1 of freely viewing monkeys." Front Syst Neurosci **7**: 1.

769 Jansen, B. H. and V. G. Rit (1995). "Electroencephalogram and Visual-Evoked Potential Generation in a
770 Mathematical-Model of Coupled Cortical Columns." Biological Cybernetics **73**(4): 357-366.
771 Jellema, T., C. H. M. Brunia and W. J. Wadman (2004). "Sequential activation of microcircuits underlying
772 somatosensory-evoked potentials in rat neocortex." Neuroscience **129**(2): 283-295.
773 Jiang, H., A. Bahramisharif, M. A. van Gerven and O. Jensen (2015). "Measuring directionality between
774 neuronal oscillations of different frequencies." Neuroimage **118**: 359-367.
775 Jirsa, V. and V. Muller (2013). "Cross-frequency coupling in real and virtual brain networks." Frontiers in
776 Computational Neuroscience **7**.
777 Kopell, N., C. Boergers, D. Pervouchine, P. Malerba and A. B. Tort (2010). Gamma and Theta Rhythms in
778 Biophysical Models of Hippocampal Circuits. Hippocampal Microcircuits:A COMPUTATIONAL MODELER'S
779 RESOURCE BOOK. V. Cutsuridis, B. Graham, S. Cobb and I. Vida, SPRINGER, 233 SPRING STREET, NEW
780 YORK, NY 10013, UNITED STATES.
781 Lakatos, P., A. S. Shah, K. H. Knuth, I. Ulbert, G. Karmos and C. E. Schroeder (2005). "An oscillatory
782 hierarchy controlling neuronal excitability and stimulus processing in the auditory cortex." Journal of
783 Neurophysiology **94**(3): 1904-1911.
784 Latora, V. and M. Marchiori (2001). "Efficient behavior of small-world networks." Physical Review Letters
785 **87**(19).
786 Lee, J. and J. Jeong (2013). "Correlation of risk-taking propensity with cross-frequency phase-amplitude
787 coupling in the resting EEG." Clin Neurophysiol **124**(11): 2172-2180.
788 Liang, X. S. (2014). "Unraveling the cause-effect relation between time series." Physical Review E **90**(5).
789 Lizier, J. T., J. Heinzle, A. Horstmann, J. D. Haynes and M. Prokopenko (2011). "Multivariate information-
790 theoretic measures reveal directed information structure and task relevant changes in fMRI
791 connectivity." J Comput Neurosci **30**(1): 85-107.

792 Lizier, J. T. and M. Prokopenko (2010). "Differentiating information transfer and causal effect." European
793 Physical Journal B **73**(4): 605-615.
794 MacKay, D. J. C. (2003). Information theory, inference, and learning algorithms. Cambridge, UK ; New
795 York, Cambridge University Press.
796 Maier, A., G. K. Adams, C. Aura and D. A. Leopold (2010). "Distinct superficial and deep laminar domains
797 of activity in the visual cortex during rest and stimulation." Front Syst Neurosci **4**.
798 McGinn, R. J. and T. A. Valiante (2014). "Phase-amplitude coupling and interlaminar synchrony are
799 correlated in human neocortex." J Neurosci **34**(48): 15923-15930.
800 Nakatani, C., A. Raffone and C. van Leeuwen (2014). "Efficiency of Conscious Access Improves with
801 Coupling of Slow and Fast Neural Oscillations." Journal of Cognitive Neuroscience **26**(5): 1168-1179.
802 Newman, M. E. J., A.-L. s. Barabási and D. J. Watts (2006). The structure and dynamics of networks.
803 Princeton, Princeton University Press.
804 Neymotin, S. A., K. M. Jacobs, A. A. Fenton and W. W. Lytton (2011). "Synaptic information transfer in
805 computer models of neocortical columns." J Comput Neurosci **30**(1): 69-84.
806 Onslow, A. C., M. W. Jones and R. Bogacz (2014). "A canonical circuit for generating phase-amplitude
807 coupling." PLoS One **9**(8): e102591.
808 Osipova, D., D. Hermes and O. Jensen (2008). "Gamma Power Is Phase-Locked to Posterior Alpha
809 Activity." Plos One **3**(12).
810 Palus, M., V. Komarek, Z. Hrncir and K. Sterbova (2001). "Synchronization as adjustment of information
811 rates: detection from bivariate time series." Phys Rev E Stat Nonlin Soft Matter Phys **63**(4 Pt 2): 046211.
812 Palus, M. and A. Stefanovska (2003). "Direction of coupling from phases of interacting oscillators: an
813 information-theoretic approach." Phys Rev E Stat Nonlin Soft Matter Phys **67**(5 Pt 2): 055201.
814 Pearl, J. (2000). Causality : models, reasoning, and inference. Cambridge, U.K. ; New York, Cambridge
815 University Press.

816 Penny, W. D., E. Duzel, K. J. Miller and J. G. Ojemann (2008). "Testing for nested oscillation." Journal of
817 Neuroscience Methods **174**(1): 50-61.
818 Pereda, E., R. Q. Quiroga and J. Bhattacharya (2005). "Nonlinear multivariate analysis of
819 neurophysiological signals." Prog Neurobiol **77**(1-2): 1-37.
820 Rubinov, M. and O. Sporns (2010). "Complex network measures of brain connectivity: Uses and
821 interpretations." Neuroimage **52**(3): 1059-1069.
822 Runge, J., J. Heitzig, N. Marwan and J. Kurths (2012). "Quantifying causal coupling strength: A lag-specific
823 measure for multivariate time series related to transfer entropy." Physical Review E **86**(6).
824 Seth, A. K., A. B. Barrett and L. Barnett (2015). "Granger causality analysis in neuroscience and
825 neuroimaging." J Neurosci **35**(8): 3293-3297.
826 Sotero, R. C. (2015). "Modeling the Generation of Phase-Amplitude Coupling in Cortical Circuits: From
827 Detailed Networks to Neural Mass Models." Biomed Res Int **2015**: 915606.
828 Sotero, R. C., A. Bortel, R. Martinez-Cancino, S. Neupane, P. O'Connor, F. Carbonell and A. Shmuel
829 (2010). "Anatomically-Constrained Effective Connectivity among Layers in a Cortical Column Modeled
830 and Estimated from Local Field Potentials." Journal of Integrative Neuroscience **9**(4): 355-379.
831 Sotero, R. C., A. B. Bortel, S. Naaman, V. M. Mocanu, P. Kropf, M. Villeneuve and A. Shmuel (2015).
832 "Laminar distribution of phase-amplitude coupling of spontaneous current sources and sinks." Frontiers
833 in Neuroscience **9**.
834 Sotero, R. C. and N. J. Trujillo-Barreto (2008). "Biophysical model for integrating neuronal activity, EEG,
835 fMRI and metabolism." Neuroimage **39**(1): 290-309.
836 Sotero, R. C., N. J. Trujillo-Barreto, Y. Iturria-Medina, F. Carbonell and J. C. Jimenez (2007). "Realistically
837 coupled neural mass models can generate EEG rhythms." Neural Computation **19**(2): 478-512.

838 Spaak, E., M. Bonnefond, A. Maier, D. A. Leopold and O. Jensen (2012). "Layer-Specific Entrainment of
839 Gamma-Band Neural Activity by the Alpha Rhythm in Monkey Visual Cortex." Current Biology **22**(24):
840 2313-2318.
841 Spiegler, A., S. J. Kiebel, F. M. Atay and T. R. Knosche (2010). "Bifurcation analysis of neural mass models:
842 Impact of extrinsic inputs and dendritic time constants." Neuroimage **52**(3): 1041-1058.
843 Stam, C. J., E. C. van Straaten, E. Van Dellen, P. Tewarie, G. Gong, A. Hillebrand, J. Meier and P. Van
844 Mieghem (2015). "The relation between structural and functional connectivity patterns in complex brain
845 networks." Int J Psychophysiol.
846 Storey, J. D. and R. Tibshirani (2003). "Statistical significance for genomewide studies." Proc Natl Acad
847 Sci U S A **100**(16): 9440-9445.
848 Szczepanski, S. M., N. E. Crone, R. A. Kuperman, K. I. Auguste, J. Parvizi and R. T. Knight (2014). "Dynamic
849 changes in phase-amplitude coupling facilitate spatial attention control in fronto-parietal cortex." PLoS
850 Biol **12**(8): e1001936.
851 Tattini, L., S. Olmi and A. Torcini (2012). "Coherent periodic activity in excitatory Erdos-Renyi neural
852 networks: The role of network connectivity." Chaos **22**(2).
853 Tort, A. B. L., R. Komorowski, H. Eichenbaum and N. Kopell (2010). "Measuring Phase-Amplitude
854 Coupling Between Neuronal Oscillations of Different Frequencies." Journal of Neurophysiology **104**(2):
855 1195-1210.
856 Tort, A. B. L., H. G. Rotstein, T. Dugladze, T. Gloveli and N. J. Kopell (2007). "On the formation of gamma-
857 coherent cell assemblies by oriens lacunosum-moleculare interneurons in the hippocampus."
858 Proceedings of the National Academy of Sciences of the United States of America **104**(33): 13490-13495.
859 Ursino, M., F. Cona and M. Zavaglia (2010). "The generation of rhythms within a cortical region: analysis
860 of a neural mass model." Neuroimage **52**(3): 1080-1094.

Valdes-Sosa, P. A., J. M. Sanchez-Bornot, R. C. Sotero, Y. Iturria-Medina, Y. Aleman-Gomez, J. Bosch-Bayard, F. Carbonell and T. Ozaki (2009). "Model Driven EEG/fMRI Fusion of Brain Oscillations." Human Brain Mapping **30**(9): 2701-2721.

Voytek, B., R. T. Canolty, A. Shestyuk, N. E. Crone, J. Parvizi and R. T. Knight (2010). "Shifts in gamma phase-amplitude coupling frequency from theta to alpha over posterior cortex during visual tasks." Front Hum Neurosci **4**: 191.

Wang, J., D. Li, X. L. Li, F. Y. Liu, G. G. Xing, J. Cai and Y. Wan (2011). "Phase-amplitude coupling between theta and gamma oscillations during nociception in rat electroencephalography." Neuroscience Letters **499**(2): 84-87.

Wang, L., Y. B. Saalmann, M. A. Pinsk, M. J. Arcaro and S. Kastner (2012). "Electrophysiological Low-Frequency Coherence and Cross-Frequency Coupling Contribute to BOLD Connectivity." Neuron **76**(5): 1010-1020.

Wang, X. J. and G. Buzsaki (1996). "Gamma oscillation by synaptic inhibition in a hippocampal interneuronal network model." Journal of Neuroscience **16**(20): 6402-6413.

Watts, D. J. and S. H. Strogatz (1998). "Collective dynamics of 'small-world' networks." Nature **393**(6684): 440-442.

Wendling, F., J. J. Bellanger, F. Bartolomei and P. Chauvel (2000). "Relevance of nonlinear lumped-parameter models in the analysis of depth-EEG epileptic signals." Biological Cybernetics **83**(4): 367-378.

White, J. A., M. I. Banks, R. A. Pearce and N. J. Kopell (2000). "Networks of interneurons with fast and slow gamma-aminobutyric acid type A (GABA(A)) kinetics provide substrate for mixed gamma-theta rhythm." Proceedings of the National Academy of Sciences of the United States of America **97**(14): 8128-8133.

Wilson, H. R. and J. D. Cowan (1972). "Excitatory and Inhibitory Interactions in Localized Populations of Model Neurons." Biophysical Journal **12**(1): 1-&.

885 Zavaglia, M., L. Astolfi, F. Babiloni and M. Ursino (2006). "A neural mass model for the simulation of
886 cortical activity estimated from high resolution EEG during cognitive or motor tasks." J Neurosci
887 Methods **157**(2): 317-329.
888 Zavaglia, M., F. Cona and M. Ursino (2010). "A neural mass model to simulate different rhythms in a
889 cortical region." Comput Intell Neurosci: 456140.

890 Barnett, L. and A. K. Seth (2011). "Behaviour of Granger causality under filtering: theoretical invariance
891 and practical application." J Neurosci Methods **201**(2): 404-419.
892 Binzegger, T., R. J. Douglas and K. A. C. Martin (2004). "A quantitative map of the circuit of cat primary
893 visual cortex." Journal of Neuroscience **24**(39): 8441-8453.
894 Bragin, A., G. Jando, Z. Nadasdy, J. Hetke, K. Wise and G. Buzsaki (1995). "Gamma (40-100-Hz) Oscillation
895 in the Hippocampus of the Behaving Rat." Journal of Neuroscience **15**(1): 47-60.
896 Brown, G., A. Pocock, M. J. Zhao and M. Lujan (2012). "Conditional Likelihood Maximisation: A Unifying
897 Framework for Information Theoretic Feature Selection." Journal of Machine Learning Research **13**: 27-
898 66.
899 Buffalo, E. A., P. Fries, R. Landman, T. J. Buschman and R. Desimone (2011). "Laminar differences in
900 gamma and alpha coherence in the ventral stream." Proc Natl Acad Sci U S A **108**(27): 11262-11267.
901 Buzsáki, G. (2006). Rhythms of the brain. Oxford ; New York, Oxford University Press.
902 Canolty, R. T., C. F. Cadieu, K. Koepsell, R. T. Knight and J. M. Carmena (2012). "Multivariate phase-
903 amplitude cross-frequency coupling in neurophysiological signals." IEEE Trans Biomed Eng **59**(1): 8-11.
904 Canolty, R. T., E. Edwards, S. S. Dalal, M. Soltani, S. S. Nagarajan, H. E. Kirsch, M. S. Berger, N. M. Barbaro
905 and R. T. Knight (2006). "High gamma power is phase-locked to theta oscillations in human neocortex."
906 Science **313**(5793): 1626-1628.
907 Canolty, R. T. and R. T. Knight (2010). "The functional role of cross-frequency coupling." Trends Cogn Sci
908 **14**(11): 506-515.

909 Carbonell, F., J. C. Jimenez, R. J. Biscay and H. De La Cruz (2005). "The local linearization method for
910 numerical integration of random differential equations." Bit Numerical Mathematics **45**(1): 1-14.
911 Cohen, M. X., C. E. Elger and J. Fell (2009). "Oscillatory activity and phase-amplitude coupling in the
912 human medial frontal cortex during decision making." J Cogn Neurosci **21**(2): 390-402.
913 Daffertshofer, A. and B. C. van Wijk (2011). "On the Influence of Amplitude on the Connectivity between
914 Phases." Front Neuroinform **5**: 6.
915 David, O. and K. J. Friston (2003). "A neural mass model for MEG/EEG: coupling and neuronal dynamics."
916 Neuroimage **20**(3): 1743-1755.
917 de Hemptinne, C., E. S. Ryapolova-Webb, E. L. Air, P. A. Garcia, K. J. Miller, J. G. Ojemann, J. L. Ostrem, N.
918 B. Galifianakis and P. A. Starr (2013). "Exaggerated phase-amplitude coupling in the primary motor
919 cortex in Parkinson disease." Proc Natl Acad Sci U S A **110**(12): 4780-4785.
920 Demiralp, T., Z. Bayraktaroglu, D. Lenz, S. Junge, N. A. Busch, B. Maess, M. Ergen and C. S. Herrmann
921 (2007). "Gamma amplitudes are coupled EEG during visual to theta phase in human perception."
922 International Journal of Psychophysiology **64**(1): 24-30.
923 Ding, M., Chen, Y., Bressler, S.L (2006). Granger causality: Basic theory and application to neuroscience.
924 Handbook of Time Series Analysis. W. Schelter. S., N., & Timmer, J. , Wiley, Wienheim.
925 Durschmid, S., T. Zaehle, K. Kopitzki, J. Voges, F. C. Schmitt, H. J. Heinze, R. T. Knight and H. Hinrichs
926 (2013). "Phase-amplitude cross-frequency coupling in the human nucleus accumbens tracks action
927 monitoring during cognitive control." Front Hum Neurosci **7**: 635.
928 Fagiolo, G. (2007). "Clustering in complex directed networks." Physical Review E **76**(2).
929 Faugeras, O., R. Veltz and F. Grimbert (2009). "Persistent neural states: stationary localized activity
930 patterns in nonlinear continuous n-population, q-dimensional neural networks." Neural Comput **21**(1):
931 147-187.

932 Florin, E. and S. Baillet (2015). "The brain's resting-state activity is shaped by synchronized cross-
933 frequency coupling of neural oscillations." Neuroimage **111**: 26-35.
934 Grimbert, F. and O. Faugeras (2006). "Bifurcation analysis of Jansen's neural mass model." Neural
935 Comput **18**(12): 3052-3068.
936 Gross, J., N. Hoogenboom, G. Thut, P. Schyns, S. Panzeri, P. Belin and S. Garrod (2013). "Speech Rhythms
937 and Multiplexed Oscillatory Sensory Coding in the Human Brain." Plos Biology **11**(12).
938 Guckenheimer, J. and P. Holmes (1997). Nonlinear oscillations, dynamical systems, and bifurcations of
939 vector fields. New York, Springer.
940 Hlavackova-Schindler, K., M. Palus, M. Vejmelka and J. Bhattacharya (2007). "Causality detection based
941 on information-theoretic approaches in time series analysis." Physics Reports-Review Section of Physics
942 Letters **441**(1): 1-46.
943 Honey, C. J., R. Kotter, M. Breakspear and O. Sporns (2007). "Network structure of cerebral cortex
944 shapes functional connectivity on multiple time scales." Proc Natl Acad Sci U S A **104**(24): 10240-10245.
945 Honey, C. J., O. Sporns, L. Cammoun, X. Gigandet, J. P. Thiran, R. Meuli and P. Hagmann (2009).
946 "Predicting human resting-state functional connectivity from structural connectivity." Proc Natl Acad Sci
947 U S A **106**(6): 2035-2040.
948 Hyafil, A., A. L. Giraud, L. Fontolan and B. Gutkin (2015). "Neural Cross-Frequency Coupling: Connecting
949 Architectures, Mechanisms, and Functions." Trends Neurosci **38**(11): 725-740.
950 Ito, J., P. Maldonado and S. Grun (2013). "Cross-frequency interaction of the eye-movement related LFP
951 signals in V1 of freely viewing monkeys." Front Syst Neurosci **7**: 1.
952 Jansen, B. H. and V. G. Rit (1995). "Electroencephalogram and Visual-Evoked Potential Generation in a
953 Mathematical-Model of Coupled Cortical Columns." Biological Cybernetics **73**(4): 357-366.
954 Jellema, T., C. H. M. Brunia and W. J. Wadman (2004). "Sequential activation of microcircuits underlying
955 somatosensory-evoked potentials in rat neocortex." Neuroscience **129**(2): 283-295.

956 Jiang, H., A. Bahramisharif, M. A. van Gerven and O. Jensen (2015). "Measuring directionality between
957 neuronal oscillations of different frequencies." Neuroimage **118**: 359-367.
958 Jirsa, V. and V. Muller (2013). "Cross-frequency coupling in real and virtual brain networks." Frontiers in
959 Computational Neuroscience **7**.
960 Kopell, N., C. Boergers, D. Pervouchine, P. Malerba and A. B. Tort (2010). Gamma and Theta Rhythms in
961 Biophysical Models of Hippocampal Circuits. Hippocampal Microcircuits:A COMPUTATIONAL MODELER'S
962 RESOURCE BOOK. V. Cutsuridis, B. Graham, S. Cobb and I. Vida, SPRINGER, 233 SPRING STREET, NEW
963 YORK, NY 10013, UNITED STATES.
964 Lakatos, P., A. S. Shah, K. H. Knuth, I. Ulbert, G. Karmos and C. E. Schroeder (2005). "An oscillatory
965 hierarchy controlling neuronal excitability and stimulus processing in the auditory cortex." Journal of
966 Neurophysiology **94**(3): 1904-1911.
967 Latora, V. and M. Marchiori (2001). "Efficient behavior of small-world networks." Physical Review Letters
968 **87**(19).
969 Lee, J. and J. Jeong (2013). "Correlation of risk-taking propensity with cross-frequency phase-amplitude
970 coupling in the resting EEG." Clin Neurophysiol **124**(11): 2172-2180.
971 Liang, X. S. (2014). "Unraveling the cause-effect relation between time series." Physical Review E **90**(5).
972 Lizier, J. T. and M. Prokopenko (2010). "Differentiating information transfer and causal effect." European
973 Physical Journal B **73**(4): 605-615.
974 MacKay, D. J. C. (2003). Information theory, inference, and learning algorithms. Cambridge, UK ; New
975 York, Cambridge University Press.
976 Maier, A., G. K. Adams, C. Aura and D. A. Leopold (2010). "Distinct superficial and deep laminar domains
977 of activity in the visual cortex during rest and stimulation." Front Syst Neurosci **4**.
978 McGinn, R. J. and T. A. Valiante (2014). "Phase-amplitude coupling and interlaminar synchrony are
979 correlated in human neocortex." J Neurosci **34**(48): 15923-15930.

980 Nakatani, C., A. Raffone and C. van Leeuwen (2014). "Efficiency of Conscious Access Improves with
981 Coupling of Slow and Fast Neural Oscillations." Journal of Cognitive Neuroscience **26**(5): 1168-1179.
982 Newman, M. E. J., A.-L. s. Barabási and D. J. Watts (2006). The structure and dynamics of networks.
983 Princeton, Princeton University Press.
984 Neymotin, S. A., K. M. Jacobs, A. A. Fenton and W. W. Lytton (2011). "Synaptic information transfer in
985 computer models of neocortical columns." J Comput Neurosci **30**(1): 69-84.
986 Onslow, A. C., M. W. Jones and R. Bogacz (2014). "A canonical circuit for generating phase-amplitude
987 coupling." PLoS One **9**(8): e102591.
988 Osipova, D., D. Hermes and O. Jensen (2008). "Gamma Power Is Phase-Locked to Posterior Alpha
989 Activity." Plos One **3**(12).
990 Palus, M., V. Komarek, Z. Hrncir and K. Sterbova (2001). "Synchronization as adjustment of information
991 rates: detection from bivariate time series." Phys Rev E Stat Nonlin Soft Matter Phys **63**(4 Pt 2): 046211.
992 Palus, M. and A. Stefanovska (2003). "Direction of coupling from phases of interacting oscillators: an
993 information-theoretic approach." Phys Rev E Stat Nonlin Soft Matter Phys **67**(5 Pt 2): 055201.
994 Pearl, J. (2000). Causality : models, reasoning, and inference. Cambridge, U.K. ; New York, Cambridge
995 University Press.
996 Penny, W. D., E. Duzel, K. J. Miller and J. G. Ojemann (2008). "Testing for nested oscillation." Journal of
997 Neuroscience Methods **174**(1): 50-61.
998 Pereda, E., R. Q. Quiroga and J. Bhattacharya (2005). "Nonlinear multivariate analysis of
999 neurophysiological signals." Prog Neurobiol **77**(1-2): 1-37.
1000 Rubinov, M. and O. Sporns (2010). "Complex network measures of brain connectivity: Uses and
1001 interpretations." Neuroimage **52**(3): 1059-1069.
1002 Runge, J., J. Heitzig, N. Marwan and J. Kurths (2012). "Quantifying causal coupling strength: A lag-specific
1003 measure for multivariate time series related to transfer entropy." Physical Review E **86**(6).

1004 Schreiber, T. (2000). "Measuring information transfer." Physical Review Letters **85**(2): 461-464.

1005 Seth, A. K., A. B. Barrett and L. Barnett (2015). "Granger causality analysis in neuroscience and

1006 neuroimaging." J Neurosci **35**(8): 3293-3297.

1007 Sotero, R. C. (2015). "Modeling the Generation of Phase-Amplitude Coupling in Cortical Circuits: From

1008 Detailed Networks to Neural Mass Models." Biomed Res Int **2015**: 915606.

1009 Sotero, R. C., A. Bortel, R. Martinez-Cancino, S. Neupane, P. O'Connor, F. Carbonell and A. Shmuel

1010 (2010). "Anatomically-Constrained Effective Connectivity among Layers in a Cortical Column Modeled

1011 and Estimated from Local Field Potentials." Journal of Integrative Neuroscience **9**(4): 355-379.

1012 Sotero, R. C., A. B. Bortel, S. Naaman, V. M. Mocanu, P. Kropf, M. Villeneuve and A. Shmuel (2015).

1013 "Laminar distribution of phase-amplitude coupling of spontaneous current sources and sinks." Frontiers

1014 in Neuroscience **9**.

1015 Sotero, R. C. and N. J. Trujillo-Barreto (2008). "Biophysical model for integrating neuronal activity, EEG,

1016 fMRI and metabolism." Neuroimage **39**(1): 290-309.

1017 Sotero, R. C., N. J. Trujillo-Barreto, Y. Iturria-Medina, F. Carbonell and J. C. Jimenez (2007). "Realistically

1018 coupled neural mass models can generate EEG rhythms." Neural Computation **19**(2): 478-512.

1019 Spaak, E., M. Bonnefond, A. Maier, D. A. Leopold and O. Jensen (2012). "Layer-Specific Entrainment of

1020 Gamma-Band Neural Activity by the Alpha Rhythm in Monkey Visual Cortex." Current Biology **22**(24):

1021 2313-2318.

1022 Spiegler, A., S. J. Kiebel, F. M. Atay and T. R. Knosche (2010). "Bifurcation analysis of neural mass models:

1023 Impact of extrinsic inputs and dendritic time constants." Neuroimage **52**(3): 1041-1058.

1024 Stam, C. J., E. C. van Straaten, E. Van Dellen, P. Tewarie, G. Gong, A. Hillebrand, J. Meier and P. Van

1025 Mieghem (2015). "The relation between structural and functional connectivity patterns in complex brain

1026 networks." Int J Psychophysiol.

1027 Storey, J. D. and R. Tibshirani (2003). "Statistical significance for genomewide studies." Proc Natl Acad
1028 Sci U S A **100**(16): 9440-9445.
1029 Strimmer, K. (2008). "A unified approach to false discovery rate estimation." BMC Bioinformatics **9**: 303.
1030 Szczepanski, S. M., N. E. Crone, R. A. Kuperman, K. I. Auguste, J. Parvizi and R. T. Knight (2014). "Dynamic
1031 changes in phase-amplitude coupling facilitate spatial attention control in fronto-parietal cortex." PLoS
1032 Biol **12**(8): e1001936.
1033 Tattini, L., S. Olmi and A. Torcini (2012). "Coherent periodic activity in excitatory Erdos-Renyi neural
1034 networks: The role of network connectivity." Chaos **22**(2).
1035 Tort, A. B. L., R. Komorowski, H. Eichenbaum and N. Kopell (2010). "Measuring Phase-Amplitude
1036 Coupling Between Neuronal Oscillations of Different Frequencies." Journal of Neurophysiology **104**(2):
1037 1195-1210.
1038 Tort, A. B. L., H. G. Rotstein, T. Dugladze, T. Gloveli and N. J. Kopell (2007). "On the formation of gamma-
1039 coherent cell assemblies by oriens lacunosum-moleculare interneurons in the hippocampus."
1040 Proceedings of the National Academy of Sciences of the United States of America **104**(33): 13490-13495.
1041 Ursino, M., F. Cona and M. Zavaglia (2010). "The generation of rhythms within a cortical region: analysis
1042 of a neural mass model." Neuroimage **52**(3): 1080-1094.
1043 Valdes-Sosa, P. A., J. M. Sanchez-Bornot, R. C. Sotero, Y. Iturria-Medina, Y. Aleman-Gomez, J. Bosch-
1044 Bayard, F. Carbonell and T. Ozaki (2009). "Model Driven EEG/fMRI Fusion of Brain Oscillations." Human
1045 Brain Mapping **30**(9): 2701-2721.
1046 Voytek, B., R. T. Canolty, A. Shestyuk, N. E. Crone, J. Parvizi and R. T. Knight (2010). "Shifts in gamma
1047 phase-amplitude coupling frequency from theta to alpha over posterior cortex during visual tasks."
1048 Front Hum Neurosci **4**: 191.

1049 Wang, J., D. Li, X. L. Li, F. Y. Liu, G. G. Xing, J. Cai and Y. Wan (2011). "Phase-amplitude coupling between
1050 theta and gamma oscillations during nociception in rat electroencephalography." Neuroscience Letters
1051 **499**(2): 84-87.
1052 Wang, L., Y. B. Saalmann, M. A. Pinsk, M. J. Arcaro and S. Kastner (2012). "Electrophysiological Low-
1053 Frequency Coherence and Cross-Frequency Coupling Contribute to BOLD Connectivity." Neuron **76**(5):
1054 1010-1020.
1055 Wang, X. J. and G. Buzsaki (1996). "Gamma oscillation by synaptic inhibition in a hippocampal
1056 interneuronal network model." Journal of Neuroscience **16**(20): 6402-6413.
1057 Watts, D. J. and S. H. Strogatz (1998). "Collective dynamics of 'small-world' networks." Nature
1058 **393**(6684): 440-442.
1059 Wendling, F., J. J. Bellanger, F. Bartolomei and P. Chauvel (2000). "Relevance of nonlinear lumped-
1060 parameter models in the analysis of depth-EEG epileptic signals." Biological Cybernetics **83**(4): 367-378.
1061 White, J. A., M. I. Banks, R. A. Pearce and N. J. Kopell (2000). "Networks of interneurons with fast and
1062 slow gamma-aminobutyric acid type A (GABA(A)) kinetics provide substrate for mixed gamma-theta
1063 rhythm." Proceedings of the National Academy of Sciences of the United States of America **97**(14): 8128-
1064 8133.
1065 Wilson, H. R. and J. D. Cowan (1972). "Excitatory and Inhibitory Interactions in Localized Populations of
1066 Model Neurons." Biophysical Journal **12**(1): 1-&.
1067 Zavaglia, M., L. Astolfi, F. Babiloni and M. Ursino (2006). "A neural mass model for the simulation of
1068 cortical activity estimated from high resolution EEG during cognitive or motor tasks." J Neurosci
1069 Methods **157**(2): 317-329.
1070
1071
1072 **Figure Legends**

Figure 1. Proposed neural mass model of the cortical column. A) Layer distribution of the four neuronal types. The excitatory populations are the intrinsically bursting (IB), and the regulatory spiking (RS). The inhibitory populations are low-threshold spiking (LTS) and fast spiking (FS). B) Connectivity matrix values used for coupling the 14 populations modeled. Negative values correspond to inhibitory connections.

Figure 2. Three population toy model. A) The model comprises three neuronal populations labelled as '1', '2', and '3', coloured in blue, red and green, respectively. This color legend is used across all panels in the figure. B) Connectivity matrix. C) Temporal dynamics of the three neuronal populations. D) Spectral density. E) Spectral density when substituting the sigmoid function with the linear function $S(x) = x$.

Figure 3. Causality vs correlation measures of PAC. A) Midx, ESC, cMI and TE. B) Midx, ESC, cMI and cTE when the noise is increased ($\sigma_1 = \sigma_2 = \sigma_3 = 10$).

Figure 4. Simulated temporal evolution of the postsynaptic potentials for all populations for one realization of the model. Excitatory populations are depicted in red and inhibitory ones in green.

Figure 5. Normalized spectral density (nSD) of the postsynaptic potentials shown in Figure 3 obtained by subtracting the mean of the spectral density vector and dividing by the standard deviation. Excitatory populations are depicted in red and inhibitory ones in green. nSD coloured in black show the results when the connections between populations are set to zero.

Figure 6. Laminar distribution of average LFP. A) Temporal dynamics in layers 2/3 (L2/3), 4(L4), 5(L5) and 6(L6). B) Spectral density (SD).

Figure 7. Phase-amplitude coupling (PAC) corresponding to the simulation presented in Figure 4. Non-significant values were set to zero and are depicted in white. Black dots indicate existing anatomical connections (see figure 1).

Figure 8. Exploring the parameter space for three different PAC combinations. A) Average cTE values for delta-gamma (orange), theta-gamma (green), and alpha-gamma (blue) PAC when considered 100 different values for nine different parameters: 1) a multiplying factor $\eta = 0.3:0.3:3$ controlling the global strength of the connectivity matrix ($\Gamma_{nm} = \eta\Gamma_{nm}$) , 2) the reciprocal of the time constant of RS populations ($k_{RS} = 5:5:500s^{-1}$), 3) the reciprocal of the time constant of IB populations ($k_{IB} = 5:5:500s^{-1}$), 4) the reciprocal of the time constant of LTS populations ($k_{LTS} = 5:5:500s^{-1}$), 5) the reciprocal of the time constant of FS populations ($k_{FS} = 5:5:500s^{-1}$), 6) the external input to the L4RS population ($p_5 = 10:10:1000$), 7) the external input to the L4FS population ($p_7 = 10:10:1000$), 8) the gains of the six excitatory populations ($G_E \equiv G_1 = G_2 = G_5 = G_8 = G_9 = G_{12} = 0.2:0.2:20$), and 9) the gains of the eight inhibitory populations ($G_I \equiv G_3 = G_4 = G_6 = G_7 = G_{10} = G_{11} = G_{13} = G_{14} = 0.3:0.3:30$). B) Plot of the fraction (ξ) of PAC connections that corresponded to anatomical connections versus η. C) Plot of cTE versus η. D) Average cTE values for direct and indirect PAC connections. Labels 'd', and 'i' correspond to direct and indirect PAC connections

Figure 9. The link between local topological measures and PAC. A) local clustering coefficient (C_m), B) local efficiency (E_m), C) local betweenness centrality (B_m). In all panels, labels 'd', and 'i' correspond to direct and indirect PAC connections, respectively. Populations can send and/or receive PAC interactions, or they can be not involved in the generation of PAC.

Figure 10. Amplitude-phase coupling (APC) corresponding to the simulation presented in Figures 4 and 5. Non-significant values were set to zero and are depicted in white. Black dots indicate existing anatomical connections (see figure 1).

Figure 11. Mechanisms mediating indirect PAC connections (Case I). A) Three population toy model comprising three neuronal populations labelled as '1', '2', and '3', oscillating in the theta (θ) , delta (δ), and gamma (γ) bands. B) PAC involving the phase of theta in population 1 and the amplitude of gamma in population 3 ($PAC_{\theta_1\gamma_3}$) obtained when varying the connectivity parameters between populations 1 and 2 ($c_{12} = 30{:}4{:}1000$) and between populations 2 and 3 ($c_{23} = 30{:}4{:}1000$). Panels C to R, displays the 16 predictors used in the ten models explored (table 4). S) Coefficient of determination (R^2) for the ten models explored (table 4). T) Correlation coefficient between the 16 predictors.

Figure 12. Mechanisms mediating indirect PAC connections (Case II). A) Three population toy model comprising three neuronal populations labelled as '1', '2', and '3', oscillating in the theta (θ) , beta (β), and gamma (γ) bands. B) PAC involving the phase of theta in population 1 and the amplitude of gamma in population 3 ($PAC_{\theta_1\gamma_3}$) obtained when varying the connectivity parameters between populations 1 and 2 ($c_{12} = 30{:}4{:}1000$) and between populations 2 and 3

1142 ($c_{23} = 30{:}4{:}1000$). Panels C to R, display the 16 predictors used in the ten models explored

1143 (table 4). S) Coefficient of determination (R^2) for the ten models explored (table 4). T)

1144 Correlation coefficient between the 16 predictors.

1145

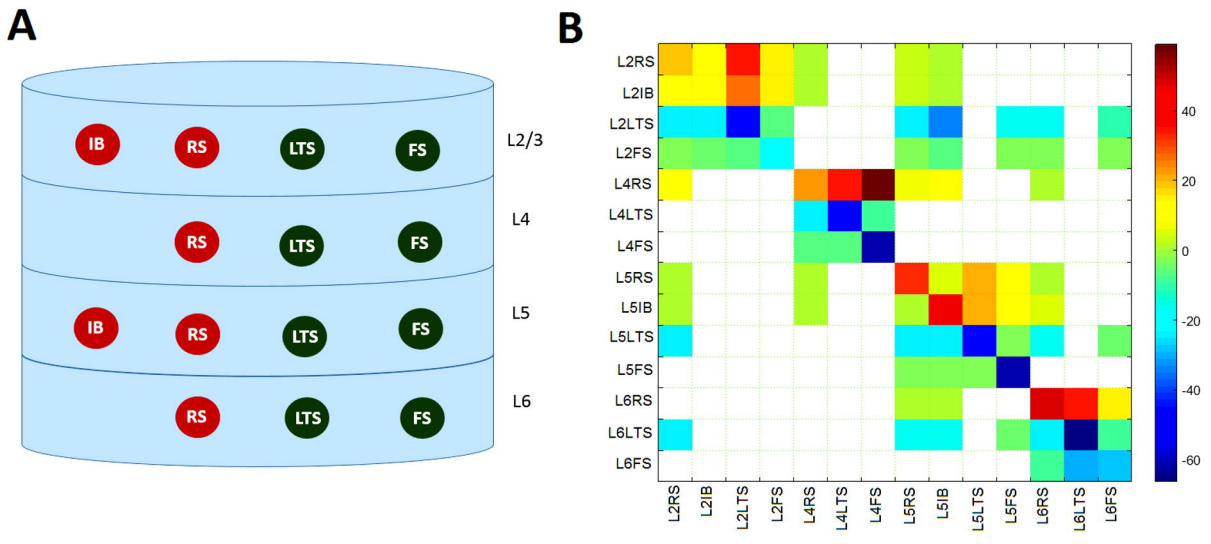
A
IB
RS
LTS
FS
L2/3
RS
LTS
FS
L4
IB
RS
LTS
FS
L5
RS
LTS
FS
L6
B
L2RS
L2IB
L2LTS
L2FS
L4RS
L4LTS
L4FS
L5RS
L5IB
L5LTS
L5FS
L6RS
L6LTS
L6FS
40
20
0
-20
-40
-60

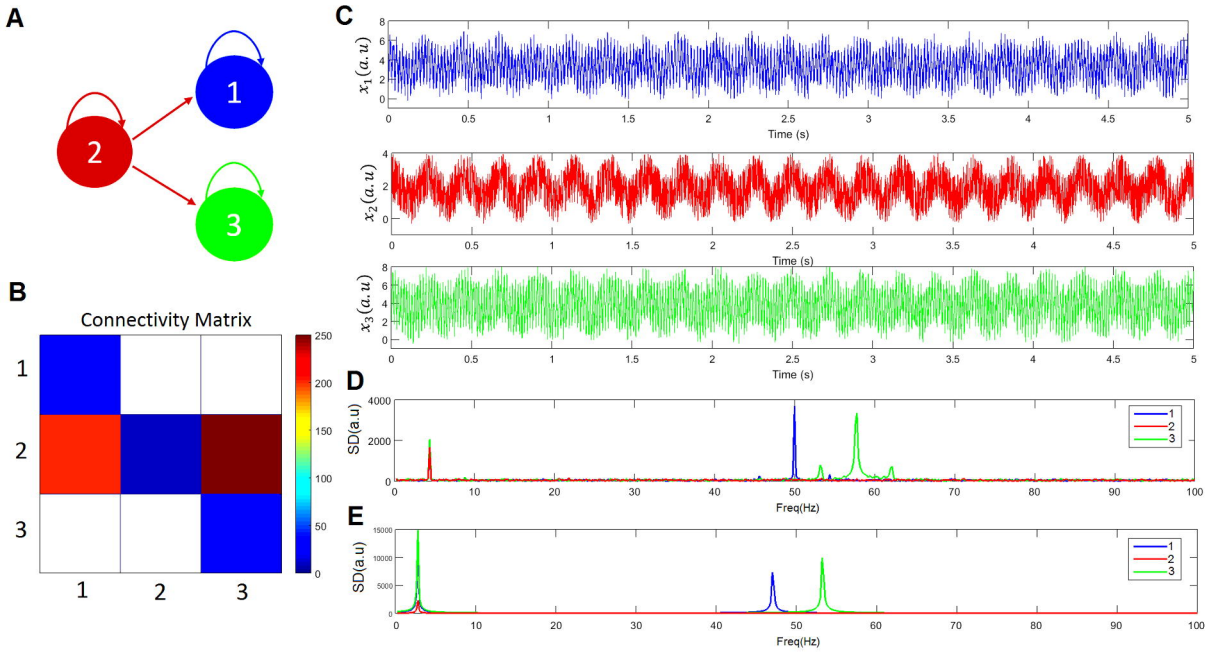
A
1
2
3
B
Connectivity Matrix
1
2
3
1
2
3
250
200
150
100
50
0
C
$x_1(a.u)$
Time (s)
$x_2(a.u)$
Time (s)
$x_3(a.u)$
Time (s)
D
SD(a.u)
Freq(Hz)
1
2
3
E
SD(a.u)
Freq(Hz)
1
2
3

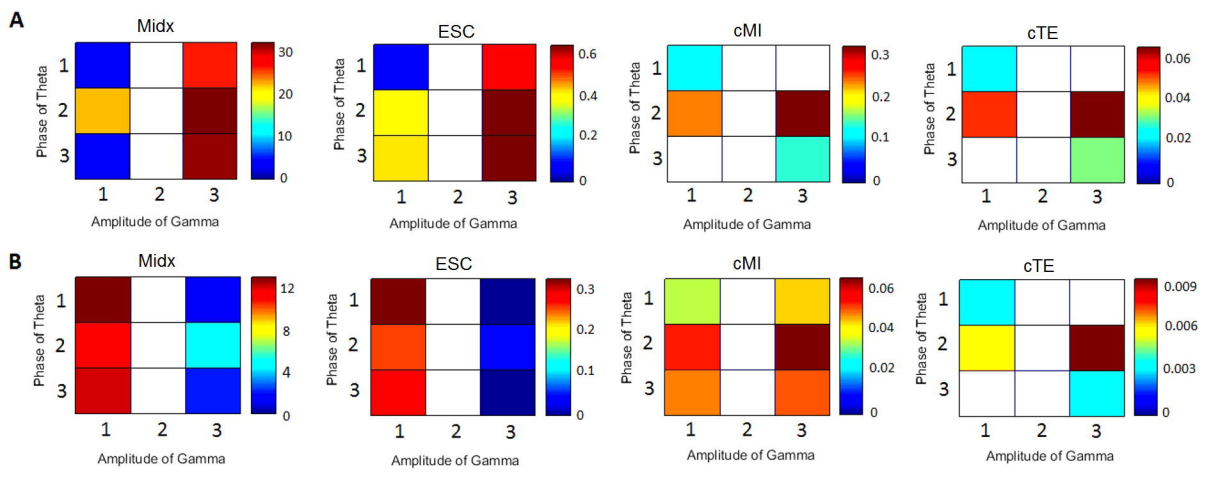
A
Midx
ESC
cMI
cTE
Phase of Theta
Amplitude of Gamma
1
2
3
30
20
10
0
0.6
0.4
0.2
0.3
0.1
0.06
0.04
0.02
B
12
8
4
0.009
0.006
0.003

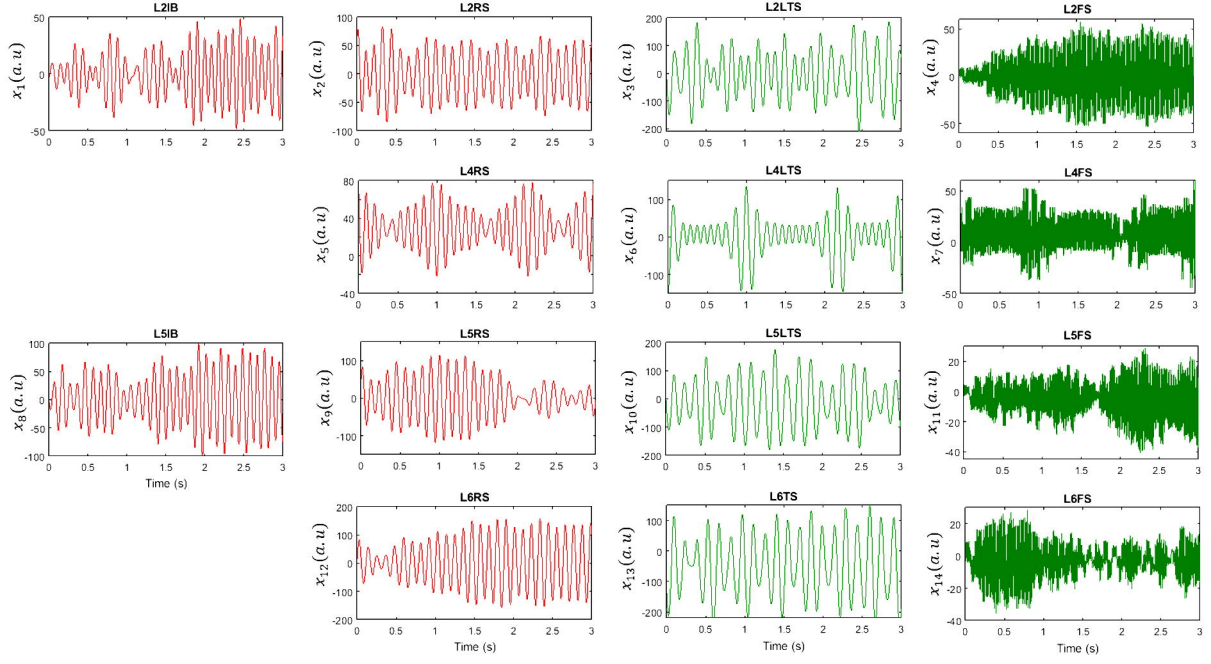
L2IB
L2RS
L2LTS
L2FS
L4RS
L4LTS
L4FS
L5IB
L5RS
L5LTS
L5FS
L6RS
L6TS
L6FS
$x_1(a.u)$
$x_2(a.u)$
$x_3(a.u)$
$x_4(a.u)$
$x_5(a.u)$
$x_6(a.u)$
$x_7(a.u)$
$x_8(a.u)$
$x_9(a.u)$
$x_{10}(a.u)$
$x_{11}(a.u)$
$x_{12}(a.u)$
$x_{13}(a.u)$
$x_{14}(a.u)$
Time (s)

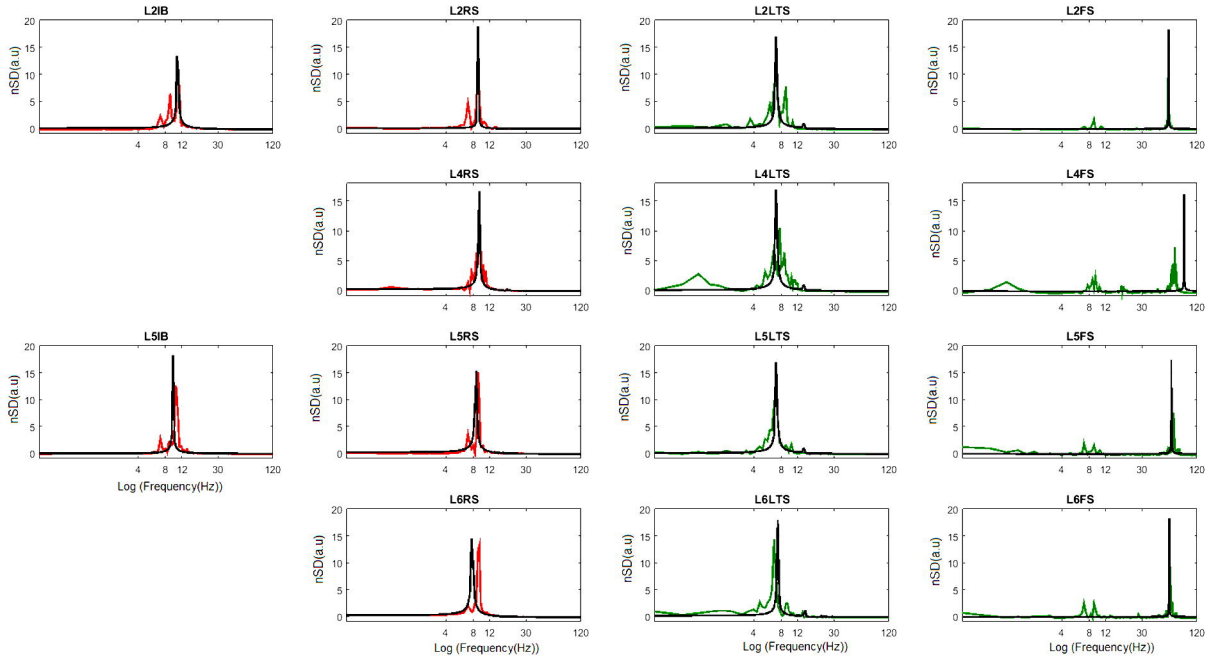
L2IB
L2RS
L2LTS
L2FS
L4RS
L4LTS
L4FS
L5IB
L5RS
L5LTS
L5FS
L6RS
L6LTS
L6FS
nSD(a.u)
Log (Frequency(Hz))
4
8
12
30
120

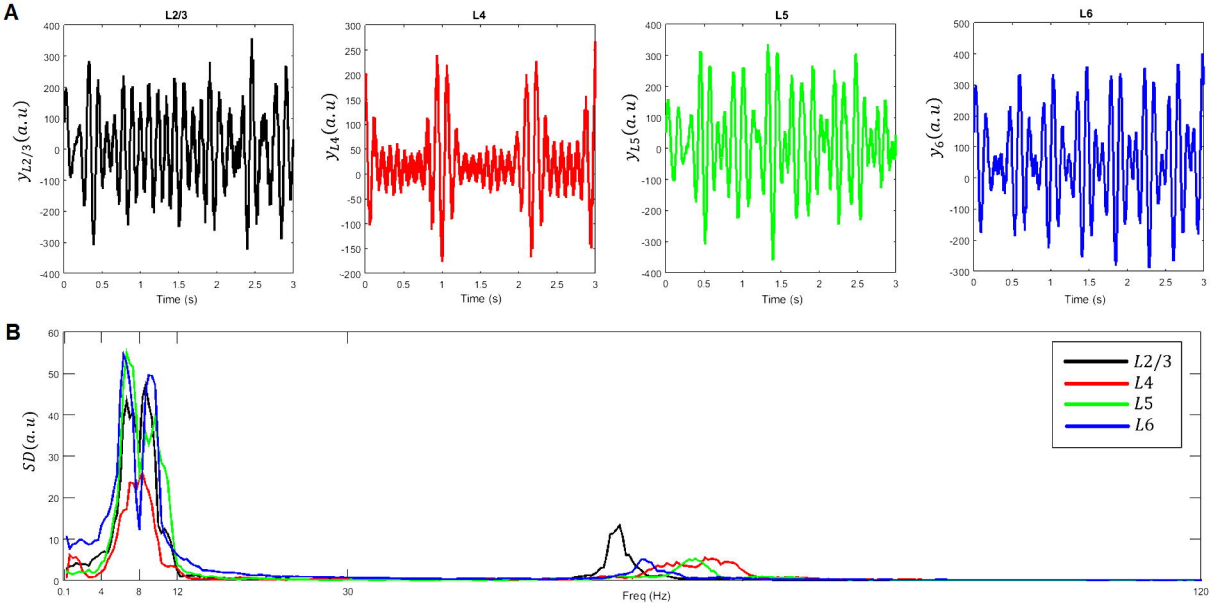
A
L2/3
L4
L5
L6
$y_{L2/3}(a.u)$
$y_{L4}(a.u)$
$y_{L5}(a.u)$
$y_6(a.u)$
Time (s)
B
$SD(a.u)$
Freq (Hz)
$L2/3$
$L4$
$L5$
$L6$

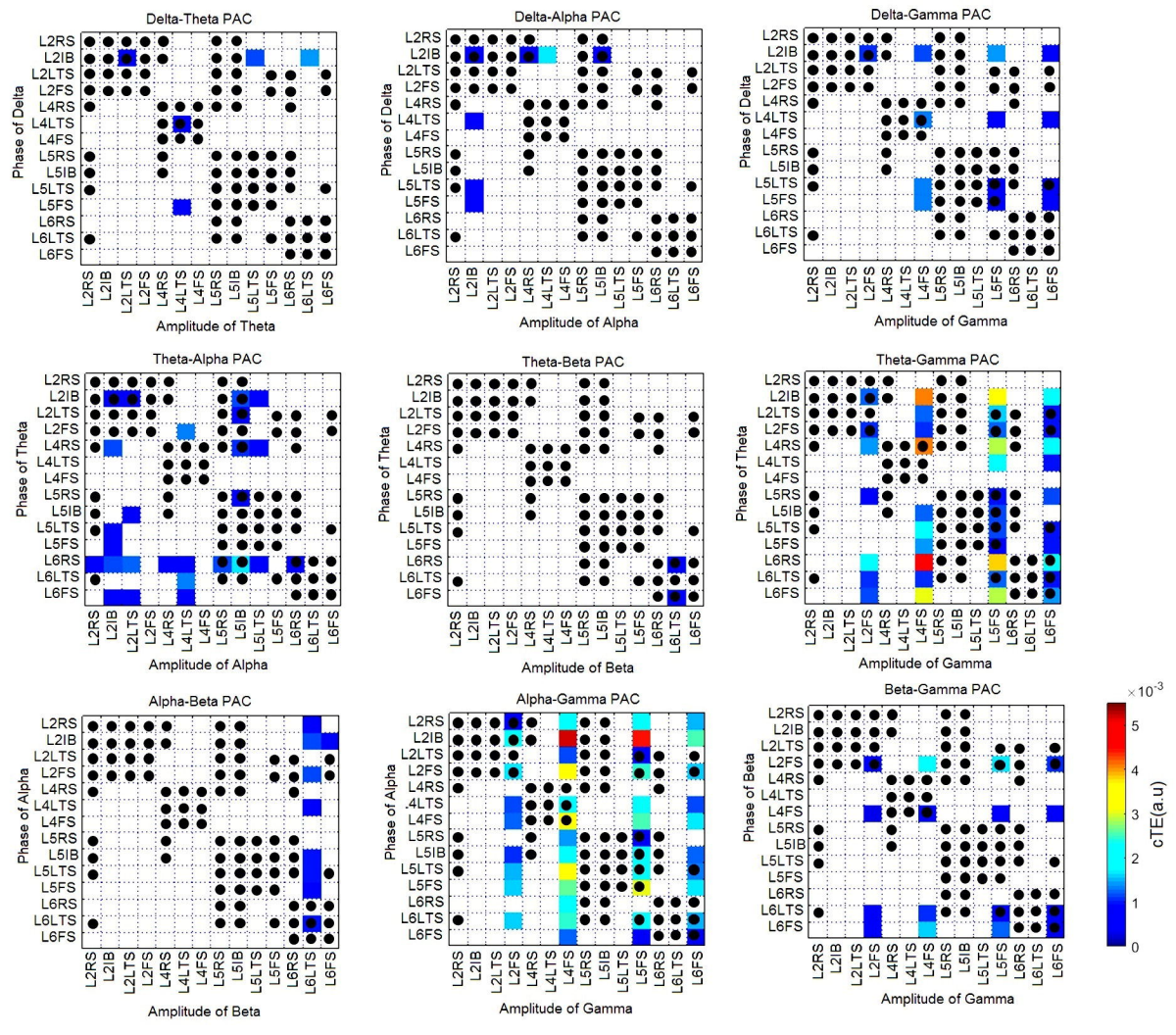
Delta-Theta PAC
Phase of Delta
Amplitude of Theta
Delta-Alpha PAC
Phase of Delta
Amplitude of Alpha
Delta-Gamma PAC
Phase of Delta
Amplitude of Gamma
Theta-Alpha PAC
Phase of Theta
Amplitude of Alpha
Theta-Beta PAC
Phase of Theta
Amplitude of Beta
Theta-Gamma PAC
Phase of Theta
Amplitude of Gamma
Alpha-Beta PAC
Phase of Alpha
Amplitude of Beta
Alpha-Gamma PAC
Phase of Alpha
Amplitude of Gamma
Beta-Gamma PAC
Phase of Beta
Amplitude of Gamma
L2RS
L2IB
L2LTS
L2FS
L4RS
L4LTS
L4FS
L5RS
L5IB
L5LTS
L5FS
L6RS
L6LTS
L6FS
×10-3
5
4
3
2
1
0
cTE(a.u)

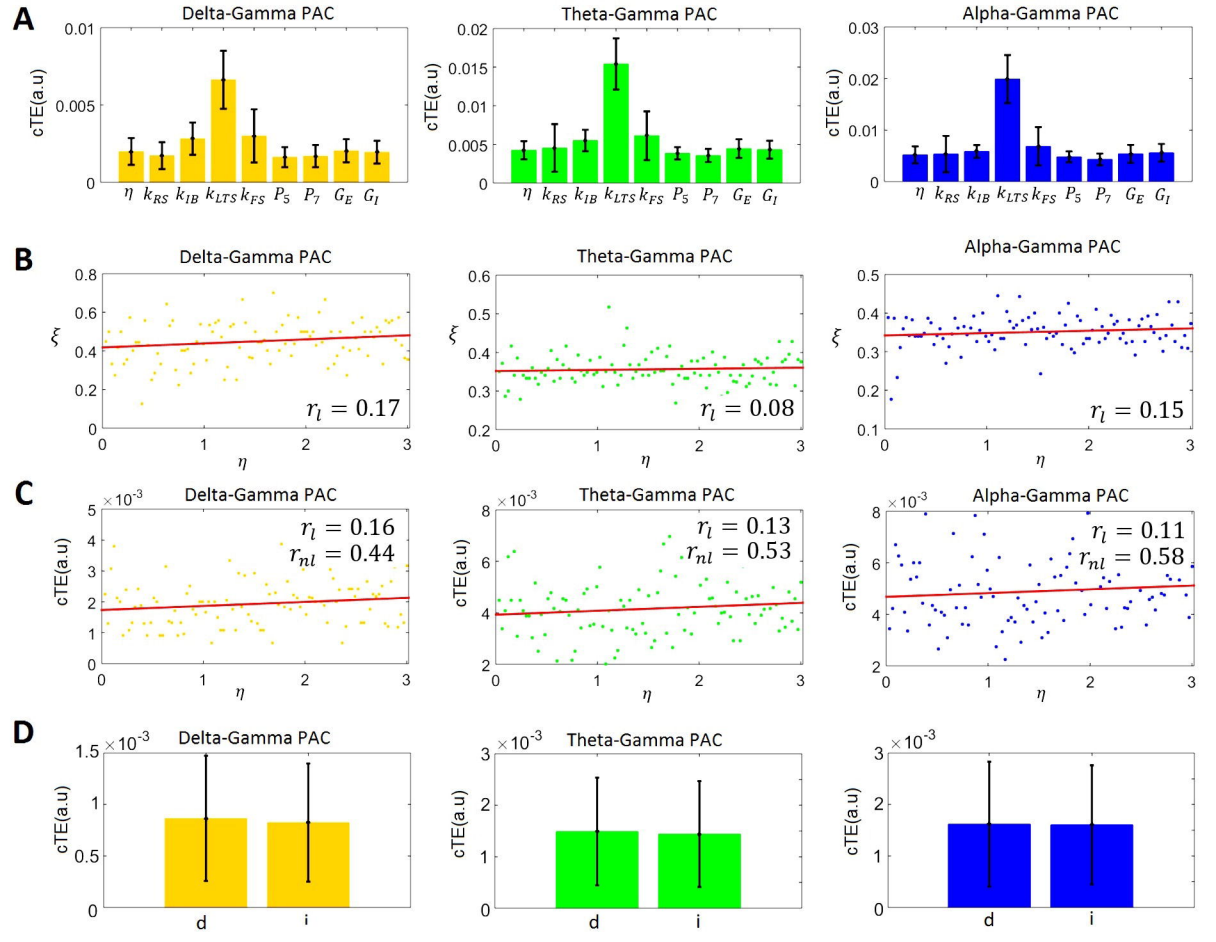
A
Delta-Gamma PAC
Theta-Gamma PAC
Alpha-Gamma PAC
cTE(a.u)
η k_{RS} k_{IB} k_{LTS} k_{FS} P_5 P_7 G_E G_I
B
Delta-Gamma PAC
Theta-Gamma PAC
Alpha-Gamma PAC
ξ
η
$r_l = 0.17$
$r_l = 0.08$
$r_l = 0.15$
C
Delta-Gamma PAC
Theta-Gamma PAC
Alpha-Gamma PAC
cTE(a.u)
η
$r_l = 0.16$
$r_{nl} = 0.44$
$r_l = 0.13$
$r_{nl} = 0.53$
$r_l = 0.11$
$r_{nl} = 0.58$
D
Delta-Gamma PAC
Theta-Gamma PAC
cTE(a.u)
d
i

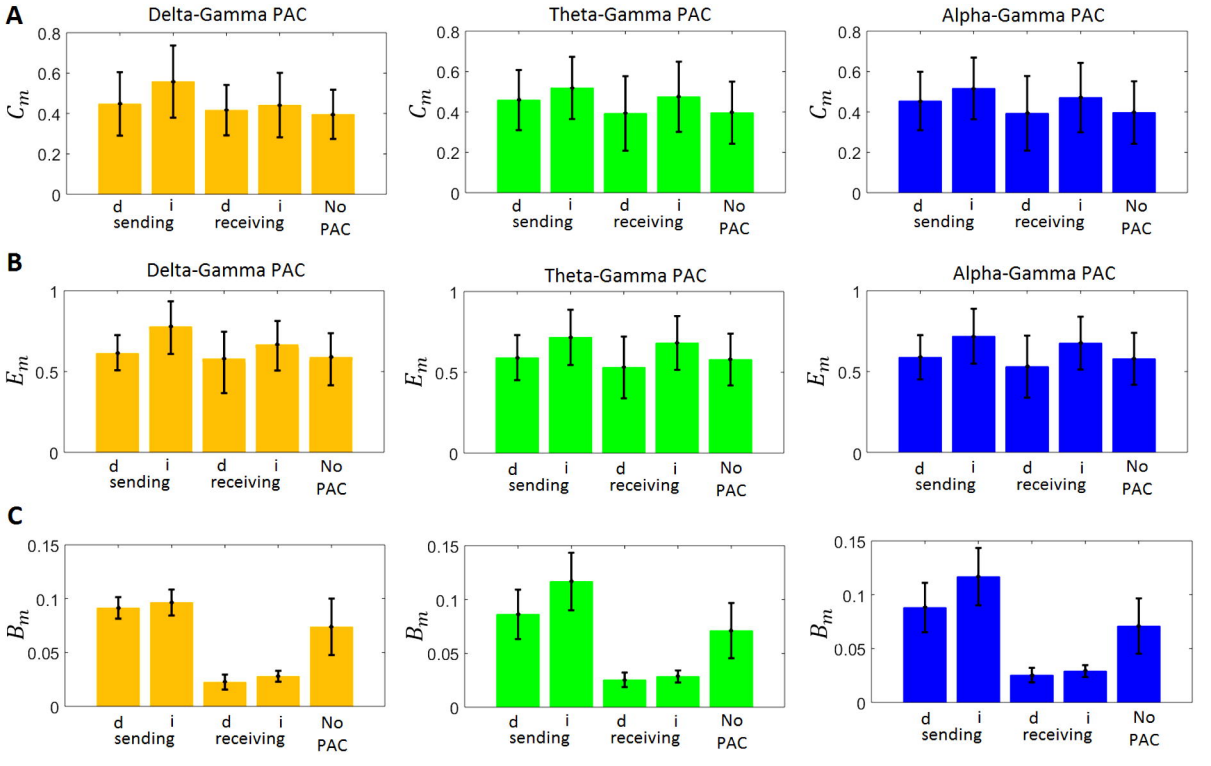
A
Delta-Gamma PAC
Theta-Gamma PAC
Alpha-Gamma PAC
C_m
0.8
0.6
0.4
0.2
0
d sending
i
d receiving
i
No PAC
B
Delta-Gamma PAC
Theta-Gamma PAC
Alpha-Gamma PAC
E_m
1
0.5
0
d sending
i
d receiving
i
No PAC
C
B_m
0.15
0.1
0.05
0
d sending
i
d receiving
i
No PAC

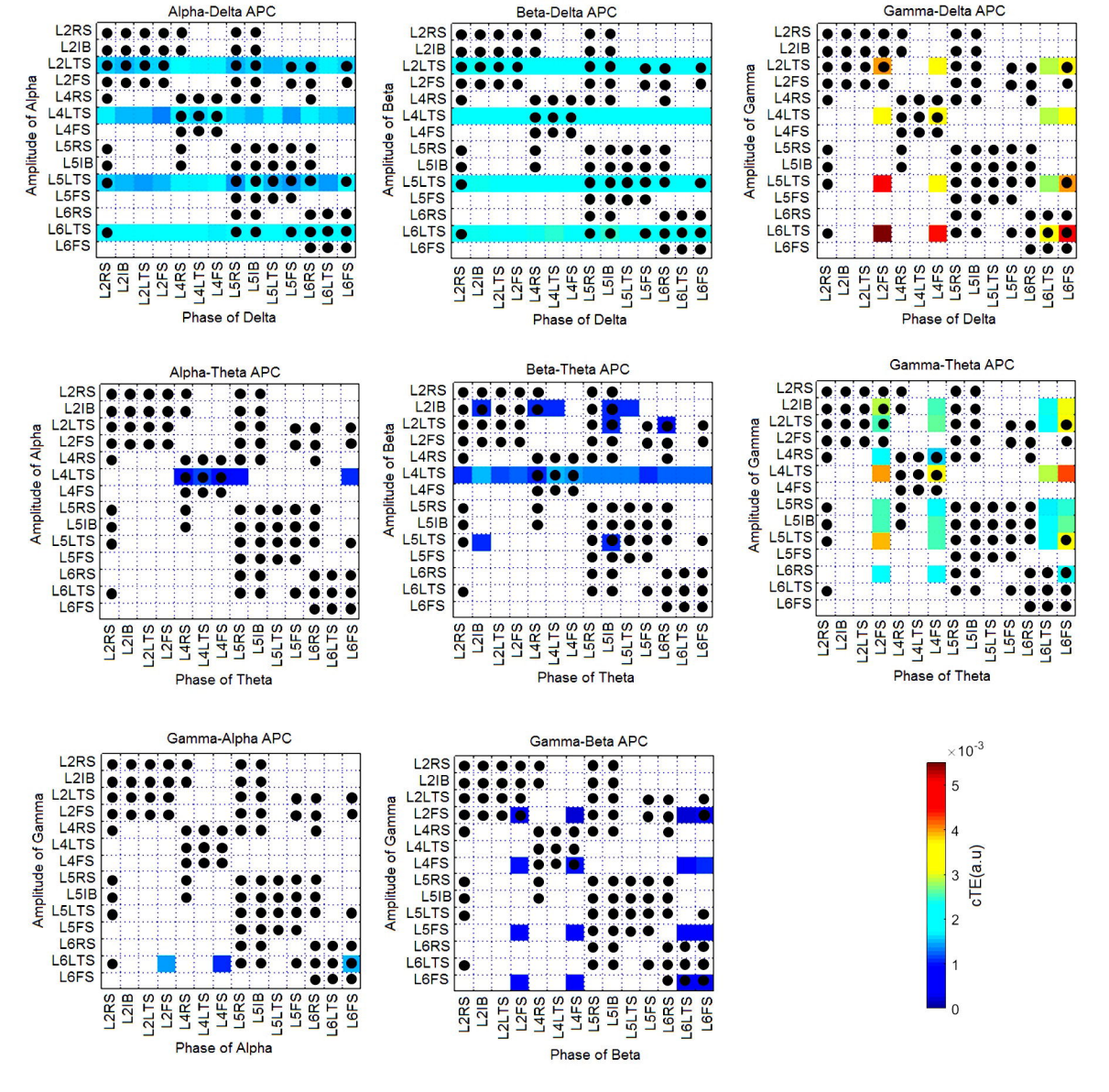
Alpha-Delta APC
Amplitude of Alpha
Phase of Delta
Beta-Delta APC
Amplitude of Beta
Phase of Delta
Gamma-Delta APC
Amplitude of Gamma
Phase of Delta
Alpha-Theta APC
Amplitude of Alpha
Phase of Theta
Beta-Theta APC
Amplitude of Beta
Phase of Theta
Gamma-Theta APC
Amplitude of Gamma
Phase of Theta
Gamma-Alpha APC
Amplitude of Gamma
Phase of Alpha
Gamma-Beta APC
Amplitude of Gamma
Phase of Beta
L2RS
L2IB
L2LTS
L2FS
L4RS
L4LTS
L4FS
L5RS
L5IB
L5LTS
L5FS
L6RS
L6LTS
L6FS
×10-3
5
4
3
2
1
0
cTE(a.u)

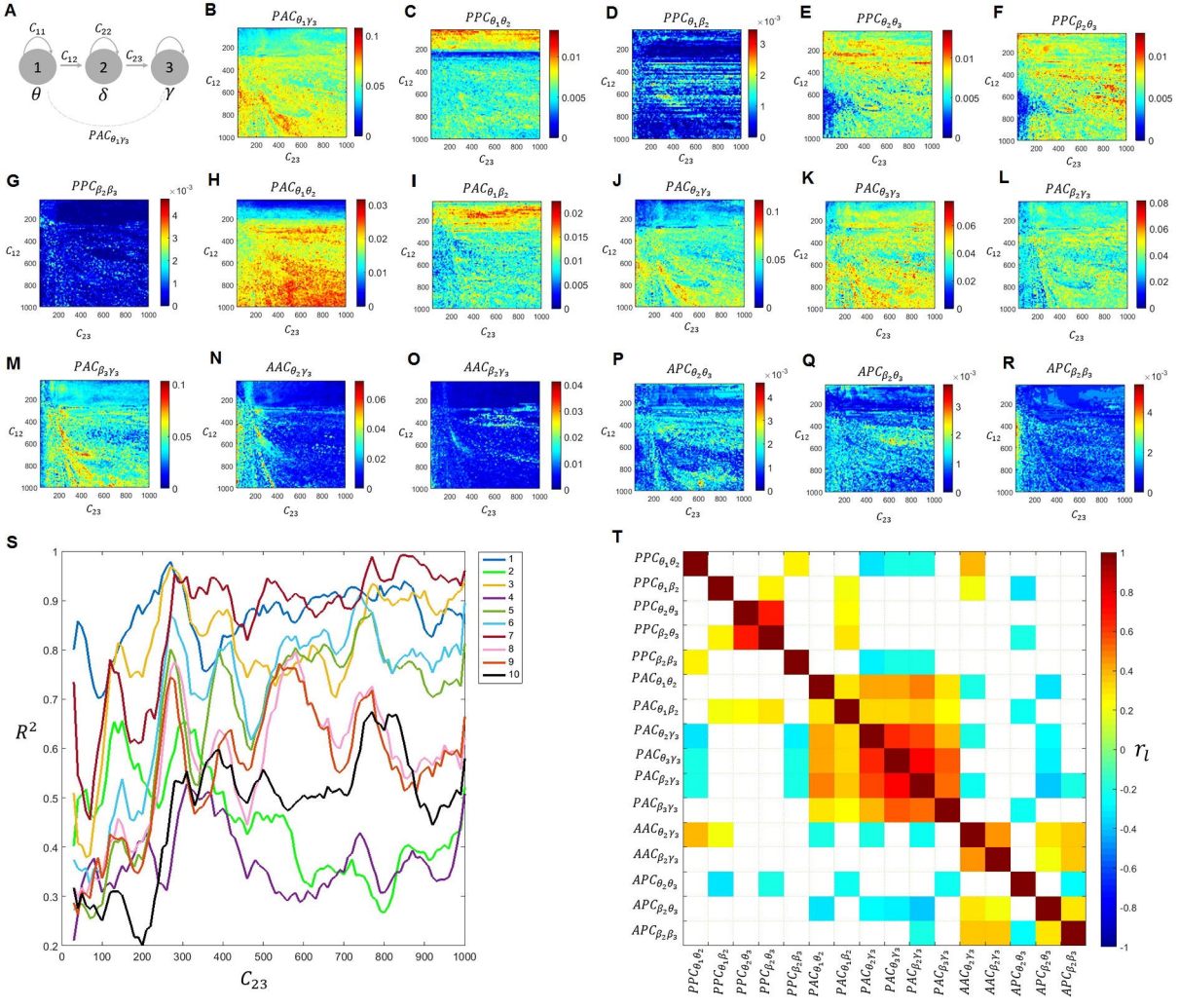
A
C_{11}
C_{22}
C_{12}
C_{23}
1
2
3
θ
δ
γ
$PAC_{\theta_1\gamma_3}$
B $PAC_{\theta_1\gamma_3}$
C $PPC_{\theta_1\theta_2}$
D $PPC_{\theta_1\beta_2}$
E $PPC_{\theta_2\theta_3}$
F $PPC_{\beta_2\theta_3}$
G $PPC_{\beta_2\beta_3}$
H $PAC_{\theta_1\theta_2}$
I $PAC_{\theta_1\beta_2}$
J $PAC_{\theta_2\gamma_3}$
K $PAC_{\theta_3\gamma_3}$
L $PAC_{\beta_2\gamma_3}$
M $PAC_{\beta_3\gamma_3}$
N $AAC_{\theta_2\gamma_3}$
O $AAC_{\beta_2\gamma_3}$
P $APC_{\theta_2\theta_3}$
Q $APC_{\beta_2\theta_3}$
R $APC_{\beta_2\beta_3}$
C_{12}
C_{23}
$\times 10^{-3}$
S
R^2
C_{23}
1
2
3
4
5
6
7
8
9
10
T
$PPC_{\theta_1\theta_2}$
$PPC_{\theta_1\beta_2}$
$PPC_{\theta_2\theta_3}$
$PPC_{\beta_2\theta_3}$
$PPC_{\beta_2\beta_3}$
$PAC_{\theta_1\theta_2}$
$PAC_{\theta_1\beta_2}$
$PAC_{\theta_2\gamma_3}$
$PAC_{\theta_3\gamma_3}$
$PAC_{\beta_2\gamma_3}$
$PAC_{\beta_3\gamma_3}$
$AAC_{\theta_2\gamma_3}$
$AAC_{\beta_2\gamma_3}$
$APC_{\theta_2\theta_3}$
$APC_{\beta_2\theta_3}$
$APC_{\beta_2\beta_3}$
r_l

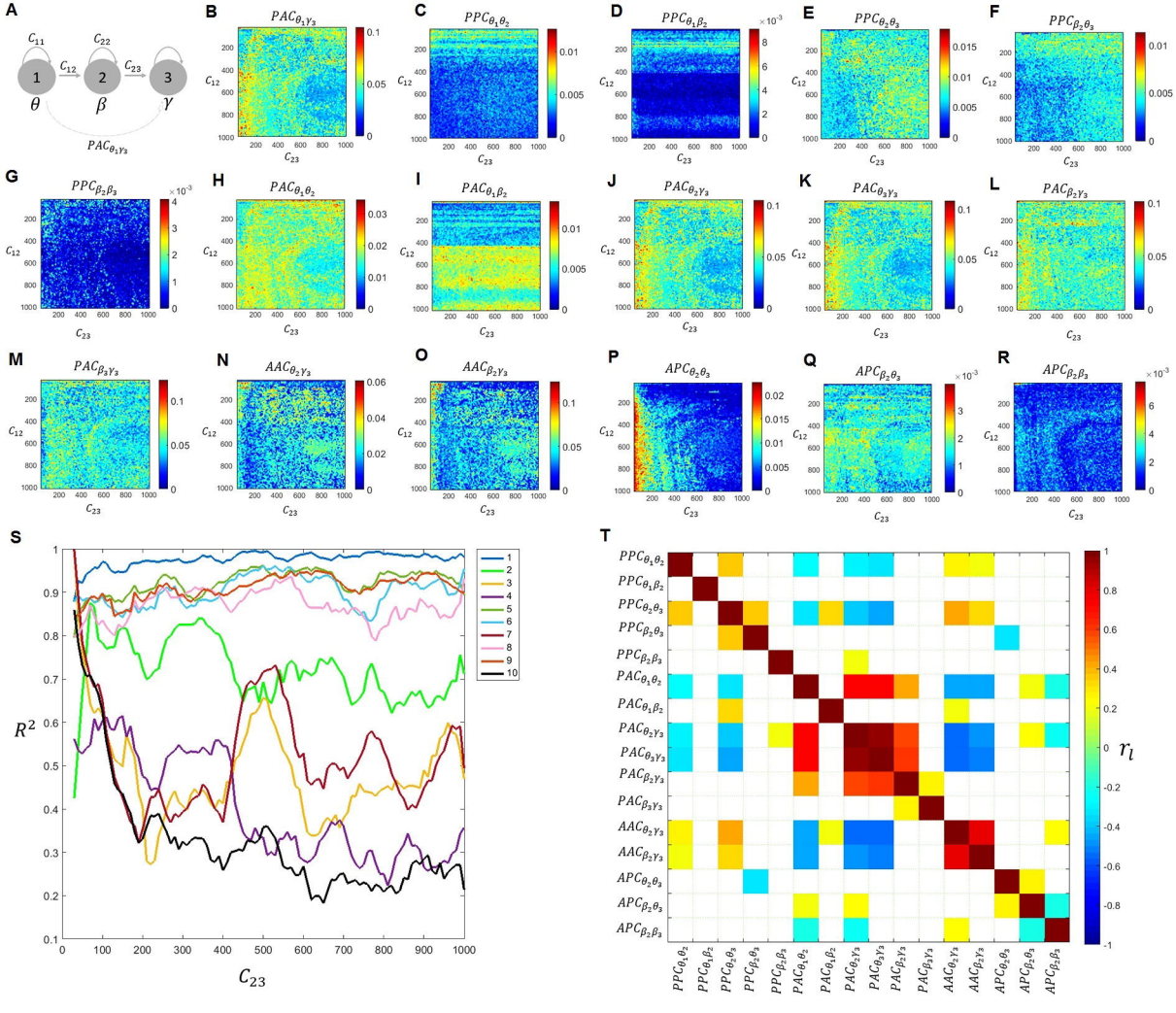
A
C_{11}
C_{22}
C_{12}
C_{23}
1
2
3
θ
β
γ
$PAC_{\theta_1\gamma_3}$
B $PAC_{\theta_1\gamma_3}$
C $PPC_{\theta_1\theta_2}$
D $PPC_{\theta_1\beta_2}$
E $PPC_{\theta_2\theta_3}$
F $PPC_{\beta_2\theta_3}$
G $PPC_{\beta_2\beta_3}$
H $PAC_{\theta_1\theta_2}$
I $PAC_{\theta_1\beta_2}$
J $PAC_{\theta_2\gamma_3}$
K $PAC_{\theta_3\gamma_3}$
L $PAC_{\beta_2\gamma_3}$
M $PAC_{\beta_3\gamma_3}$
N $AAC_{\theta_2\gamma_3}$
O $AAC_{\beta_2\gamma_3}$
P $APC_{\theta_2\theta_3}$
Q $APC_{\beta_2\theta_3}$
R $APC_{\beta_2\beta_3}$
C_{12}
C_{23}
S
R^2
C_{23}
1
2
3
4
5
6
7
8
9
10
T
$PPC_{\theta_1\theta_2}$
$PPC_{\theta_1\beta_2}$
$PPC_{\theta_2\theta_3}$
$PPC_{\beta_2\theta_3}$
$PPC_{\beta_2\beta_3}$
$PAC_{\theta_1\theta_2}$
$PAC_{\theta_1\beta_2}$
$PAC_{\theta_2\gamma_3}$
$PAC_{\theta_3\gamma_3}$
$PAC_{\beta_2\gamma_3}$
$PAC_{\beta_3\gamma_3}$
$AAC_{\theta_2\gamma_3}$
$AAC_{\beta_2\gamma_3}$
$APC_{\theta_2\theta_3}$
$APC_{\beta_2\theta_3}$
$APC_{\beta_2\beta_3}$
r_l